Ore Geology Reviews 101 (2018) 330–348

Contents lists available at ScienceDirect

Ore Geology Reviews

journal homepage: www.elsevier.com/locate/oregeorev

Metamorphic evolution of sulphide-rich chromitites from the Chernichevo ultramafic massif, SE Bulgaria

José M. González-Jiménez[a,*], Vanessa Colás[b], Fernando Gervilla[a,c], Thomas N. Kerestedjian[d], Ivanina Sergeeva[d], Andrea Casado-González[a], Isabel Fanlo[e]

[a] Departamento de Mineralogía y Petrología, Facultad de Ciencias, Universidad de Granada, Avda. Fuentenueva s/n, 18002 Granada, Spain
[b] Instituto de Geología, Universidad Nacional Autónoma de México, Ciudad Universitaria, 04510 Ciudad de México, Mexico
[c] Instituto Andaluz de Ciencias de la Tierra (IACT), CSIC-UGR, Avda. de las Palmeras 4, 18100 Armilla, Granada, Spain
[d] Geological Institute, Bulgarian Academy of Sciences, 24 Georgi Bonchev Str., 1113 Sofia, Bulgaria
[e] Departamento de Ciencias de la Tierra, Cristalografía y Mineralogía, Universidad de Zaragoza, Pedro Cerbuna 12, 50009 Zaragoza, Spain

ARTICLE INFO

Keywords:
Chromite
Sulphide
Trace-elements
EBSD
Rhodope Metamorphic Complex
PGE remobilization

ABSTRACT

The upper mantle rocks of the metamorphosed ophiolite of Chernichevo, Rhodope Metamorphic Complex in southern Bulgaria, host small chromite ores with unusual mineralization of base-metal sulphides rich in platinum-group elements. Mineralogical and chemical data indicate that after their formation in the mantle the Chernichevo's chromite ores were modified by the intrusion of an alkaline mafic melt, which resulted in the precipitation of a suite of metasomatic minerals (sulphides, calcite, apatite and ilmenite), accompanied by an increase in FeO, TiO_2, Ga, Zn, Vn, Mn, and especially Ti and Fe_2O_3 contents in the chromite. The degree of chemical modification and abundance of metasomatic minerals are positively correlated and mark the extent of reaction of the chromitite with the intruding melt. Sulphide segregation promoted the concentration of high amounts of PGEs (up to 3661 ppb), particularly Pt and Pd, yielding chromite ores with a typical flat to positive-sloped chondrite-normalized pattern. Subsequently, the chromite ores were deformed and metamorphosed together with their host rocks at ultra-high pressure (UHP) (> 2.5 GPa, > 1200 °C) to be later retrograded under eclogite and finally hydrous amphibolite-facies conditions, giving rise to three microstructural types. Metamorphism of the most metasomatized (i.e., sulphide-rich) chromitites at temperatures > 700 °C within the conditions of UHP and eclogite-facies resulted in the formation of (1) *non-porous recrystallized chromite*, consisting of a granoblastic microstructure made-up of coarse-grained blasts and finer-grained chromite neoblasts. In contrast, hydrous metamorphism on the less metasomatized (i.e., sulphide-poor) chromitite under the conditions of amphibolite-facies (ca. 482–483 °C) resulted in the formation of (2) *partly altered chromite*, characterized by unaltered cores surrounded by Fe^{2+}-rich and Al-depleted porous chromite containing abundant clinochlore, and (3) *porous chromite* corresponding to a chromite that was entirely transformed by the metamorphic alteration to Fe^{2+}-rich and Al-depleted porous chromite. During metamorphism magmatic Ni-Fe-Cu sulphides originally formed during the metasomatic event in the mantle were altered, resulting in a major leaching of Cu-rich sulphides, leading to significant remobilization of Pt and Pd.

1. Introduction

Chromitites hosted in the shallow portions of the oceanic upper mantle usually crystallize from arc-type melts that are typically S-undersaturated (e.g., Prichard et al., 2008; González-Jiménez et al., 2012). This hampers the segregation of immiscible sulphide melts at the high temperatures of chromite crystallization and subsequently the formation of sulphide mineralization, a key process for the concentration of noble metals in mineable concentrations (Naldrett, 2010; O'Driscoll and González-Jiménez 2016). Thus, magmatic Fe-Ni-Cu sulphides have only been described as disseminated (1–3 vol%) in some chromite-rich rocks (including dunites and chromitites) in the mantle section of a few ophiolites, including Unst (Shetland; Prichard and Lord, 1993; Derbyshire et al., 2013), Acoje (Philippines, Bacuta et al., 1990) and northern Oman (Neigishi et al., 2013). In these ophiolites, Fe-Ni-Cu sulphides were found a inter-cumulus to chromite grains indicating that sulphide saturation was achieved after chromite formation, very likely after long-term cooling and/or fractionation of the parental (ultra)-

* Corresponding author.
E-mail address: jmgonzj@ugr.es (J.M. González-Jiménez).

https://doi.org/10.1016/j.oregeorev.2018.07.024
Received 21 May 2018; Received in revised form 16 July 2018; Accepted 25 July 2018
Available online 27 July 2018

mafic melt. Proenza et al. (2001) reported a peculiar type of chromite ore with up to 5 vol% of Fe-Ni-Cu sulphides, located at the contact between typical podiform chromitite and pegmatitic olivine-norite dikes in the Pososi Mine (Moa-Baracoa Ophiolite, eastern Cuba). In this unique case, the immiscible segregation of sulphide liquid was produced by the interaction between already formed chromitite and the intruding volatile-rich silicate melt parental of the olivine-norite dikes. Moreover, masses of Fe-Ni-Cu sulphides have been found associated with chromitites from Eretria in Greece, although these have been interpreted as precipitated from hydrothermal fluids related to serpentinization of the host ultramafic rocks (Economou and Naldrett, 1984).

In this paper we performed a detailed study of the mineralogy, microstructure and geochemistry of sulphide-rich chromite ores hosted in the mantle section of the Chernichevo ophiolite in the Rhodope Metamorphic Complex, southern Bulgaria (Colás et al., 2014). This "meta-ophiolite" that experienced a complex metamorphic history gives us an unprecedented opportunity to evaluate the impact of metamorphism on magmatic Fe-Ni-Cu sulphides associated with mantle-hosted chromitites. We present and discuss whole-rock PGE data of the chromitite as well as novel EPMA and LA-ICPMS in situ analysis on individual grains of oxides (chromite, magnetite and ilmenite), phosphates, silicates and sulphides to fingerprint the igneous, metasomatic and metamorphic signals. In addition, crystallographic orientation maps of single chromite grains, obtained using the Electron-Backscattered Secondary Diffraction (EBSD) technique, were collected to constrain the micro-structural relations between deformation and alteration at the scale of small chromite grains. Finally, these results are used to construct an integrate model for the evolutionary history of the sulphide-rich chromitite ores. Our results provide clues on the interplay between deformation and fluid/melt infiltration in the remobilization of precious metals during regional metamorphism of ultramafic rocks.

2. Geological setting

2.1. The Eastern Rhodope complex

The Chernichevo ultramafic massif is located near the village of Chernichevo in southern Bulgaria, approximately 5 km north of the Bulgaria-Greece border (Fig. 1a–c; Kolcheva et al., 2000). Geologically it belongs to the Byala Reka unit, occupying the rim of the Byala Reka dome (Ivanov, 2000), one of two late-Alpine extensional metamorphic domes that form the larger-scale domal structure of the Eastern Rhodope Metamorphic Core Complex: the Kesebir-Kardamos to the west and Byala Reka-Kechros to the east respectively (Fig. 1b; Kolcheva et al., 2000; Bonev, 2006).

The Eastern Rhodope, together with the West and Central Rhodope form a 300 × 300 km open NW-SE trending antiform formed during the Alpine Orogeny between the Balkan Belt to the north and the Dinarides-Hellenides to the south-southwest (Fig. 1a; Collings, 2014 and references therein). The Rhodope Metamorphic Core Complex comprises high-grade metamorphic rocks of Paleozoic age that were intruded by unmetamorphosed Late Cretaceous and Miocene granitoids (Liati and Gebauer, 1999; Peytcheva et al., 2004; Bonev, 2006; Turpaud and Reischmann, 2010; Janák et al., 2011; Jahn-Awe et al., 2010; Collings, 2014) and covered by widespread Tertiary sedimentary, volcano-sedimentary and volcanic rocks (Bonev et al., 2010 and references therein). Nowadays, this metamorphic core complex is regarded as a south directed nappe complex formed as a result of a north dipping Cretaceous subduction zone associated with the closure of the Vardan Ocean (Ricou et al., 1998). The nappe had experienced post orogeny extension during the Late Eocene-Miocene leading to the emplacement of a series of large-scale metamorphic domes (core complexes) that dominate the regional geology (Burg et al., 1996; Bonev et al., 2010; Nagel et al., 2011).

For the sake of clarity, the high-grade metamorphic rocks that constitute the Rhodope Metamorphic Core Complex have been collectively grouped into two main units (upper and lower). These two units crop out in different parts of the large-scale domal structure along the West, Central and Eastern Rhodope (Bonev, 2006). In the Eastern Rhodope where the Chernichevo ultramafic body crops out, the lower unit is restricted to the core of the dome structures, forming the footwall of a detachment fault system that is easily identified at outcrop scale. This hanging wall that corresponds to the *autochthonous core* is known in the literature as the Gneiss-Migmatite Complex (Kozhoukharov et al., 1988; Haydoutov et al., 2001), the Lower High-Grade Unit (Bonev, 2006) or the Lower Allochthon (Janák et al., 2011). The rocks of this lower unit are orthogneisses (intercalated with migmatites and migmatitic gneisses, psammitic paragneisses, metapelites and scarce amphibolites) and metagranites. Pressure-temperature conditions estimated for the metamorphism of the Paleozoic paragneisses

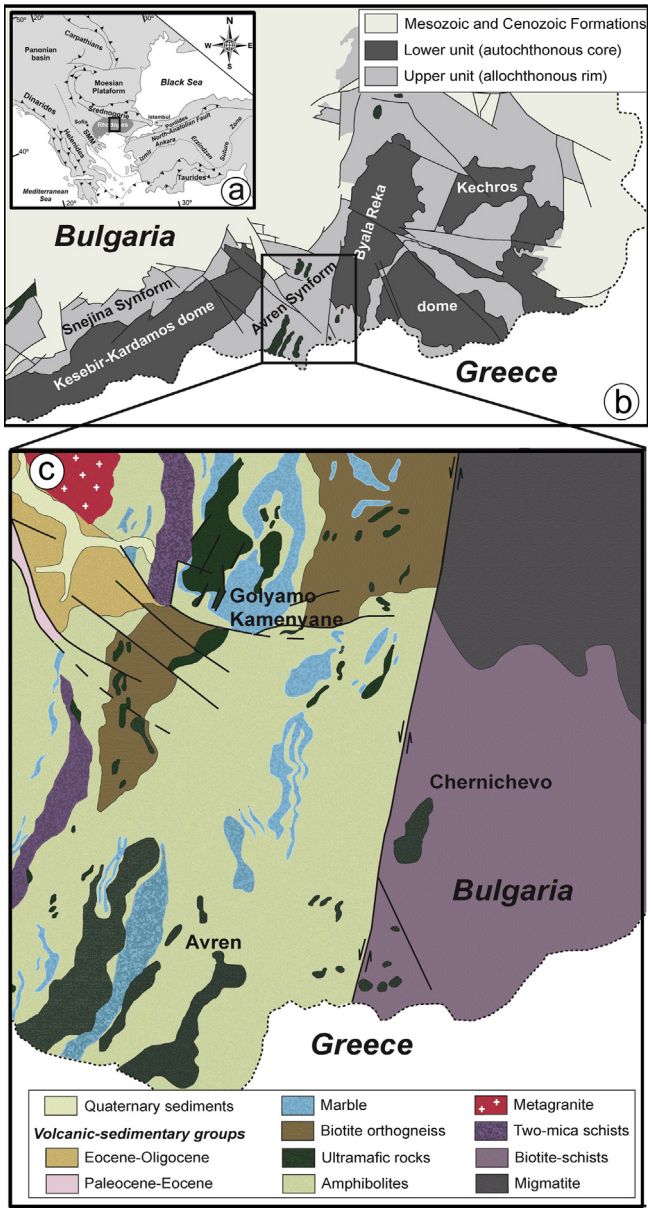

Fig. 1. (a) Geographical location of the Rhodope Metamorphic Core Complex in the tectonic frame of south-eastern Europe (after Marchev et al., 2005). (b) and (c) geological map of the eastern part of Rhodope in south Bulgaria showing the localization of the Chernichevo ultramafic body. These maps are compilations after Bonev (2006), Haydoutov et al. (2004) and 1:50,000 map of Bulgaria [sheets K35-88 V and K35-88-G, Sarov et al. (2004)]. Legends are in all cases inset in the figures.

and metapelites indicated eclogite facies (1.3–2.2 GPa 500–600 °C) followed by variable retrogressive P-T trajectories (depending on authors: Mposkos and Liati, 1993; Mposkos, 1998; Mposkos et al., 2012) down to greenschist-facies conditions. The upper unit or *allochthonous rim* of the domal structure is known as the Variegated Complex (Kozhoukharov et al., 1988; Haydoutov et al., 2001, 2004), the upper High-Grade Unit (Bonev, 2006) or the Upper Allochthon (Janák et al., 2011). This upper unit is more heterogeneous than the lower one and comprises intercalated meta-igneous (metagabbros and ortho-amphibolites) and metasedimentary rocks (para-amphibolites, marbles, metapelitic schist, paragneisses) of mixed continental and oceanic affinity (Haydoutov et al., 2004). This unit also includes widespread bodies of ultramafic rocks (upper mantle harzburgite-dunite, cumulate dunite-orthopyroxenite and cumulated dunite-wehrlite-clinopyroxenite), which were deformed and metamorphosed together with the surrounding metamorphic rocks (Kozhoukharova, 1985; Haydoutov et al., 2004). These ultramafic rocks that may preserve garnet-bearing assemblages (Mposkos, 2002) are regarded, together with metavolcanic and metasedimentary rocks, as fragments of an ophiolite (i.e., the Rhodopean Ophiolite Association; Kozhoukharova, 1985, 1996; Haydoutov et al., 2004, Kozhoukharova, 2010).

2.2. The Chernichevo ultramafic massif

The Chernichevo ultramafic massif is a lens-like small ultramafic body 2 × 0.5 km (total exposed area ~1 km^2) trending NE-SW (Fig. 1c). This ultramafic body that is included within staurolite-bearing micaschists consists of metaharzburgite and metadunite hosting chromitite bodies and topped by a sequence of metagabbros at the base of the crust near the mantle-crust transition (Colás et al., 2014). Although the metamorphic conditions of the Chernichevo ultramafic massif have not yet been calculated, in the neighboring immediately to the west Avren synform there are eclogites retrograded to amphibolite that record a wide range of P-T conditions: 1.7–1.2 GPa and 811–750 °C (Kozhoukharova, 1998), 1.2–0.8 GPa and 700–650 °C (Mogessie et al., 2008) and 1.2–1 GPa and 520–440 °C (Mukasa et al., 2003). Haydoutov et al. (2004) have reported similar P-T conditions (1.1–0.5 GPa and 780–680 °C) in metagabbros associated with the Bubino ultramafic body (north of Chernichevo) but lower pressures in ortho-amphibolites from the eastern side of the Avren synform (0.2–0.5 GPa ad 630–520 °C) (Fig. 1b). Moreover, metaperidotites from the Kimi Complex (the Greek equivalent of the Avren synform in Bulgaria) record evidence of ultra-high pressure (UHP)/high temperature (HT) metamorphism (> 2.5 GPa and > 1200 °C), with a later overprinting in eclogite- or granulite-facies (1.6–1.4 GPa and 775–750 °C) (Mposkos, 2002; Mposkos and Krohe 2000, 2006; Liati and Gebauer, 2001). A final retrogression in the PT conditions of amphibolites (~1 GPa and 650–600 °C) is also recorded in metasediments spatially associated with these mantle rocks (Mposkos and Krohe, 2000, 2006; Mposkos, 2002). Mposkos et al. (2012) have estimated a somewhat similar retrograde metamorphic pathway in the rocks of the Gneiss–Migmatite Complex: from ultra-high pressures (2.3–2.1 GPa) but lower temperatures (617–553 °C), to eclogite facies (1.8–1.5 GPa and 672–566 °C), with amphibolite-facies overprint (0.8–0.6 GPa and 570–498 °C).

3. Analytical methods

Analytical procedures are described in detail in the electronic Digital Appendix 1, and the results are presented in electronic Digital Appendices from 2 to 10.

4. Chromite ore description

4.1. Chromitite outcrops and textures

Three small podiform-like chromitite bodies (with lengths of a few meters and thicknesses between 0.5 m and 2 m; Colás et al., 2014) are exposed in the Chernichevo ultramafic massif. They are hosted within a variable thick horizon of metadunite, which is concordant with the foliation of the host metaharzburgites. The chromitite bodies consist of semi-massive (60–85 vol% chromite), and to a lesser extent massive (> 85% chromite) textures. These chromitites were significantly altered by metamorphism (Fig. 2a–d), which has produced two of the four types of metamorphic microstructures in chromite as defined by Gervilla et al. (2012) for metamorphosed chromite ores in the nearby Golyamo Kamenyane serpentinite body: (1) partly altered chromite and (2) porous chromite. Both types of microstructures were found in samples of semi-massive chromitites, although the latter ones predominate in those samples with the lowest modal volume of chromite. *Partly altered chromite* is characterized by unaltered cores surrounded by porous chromite with abundant inclusions of clinochlore (Fig. 2a). Clinochlore also fills the pores of *porous chromite* corresponding to a chromite that was entirely transformed by metamorphic alteration (Fig. 2b). These two types of microstructures are made up of subhedral to anhedral chromite crystals (up to of 0.1–0.5 cm across) with clinochlore forming the interstitial matrix between chromite grains. These chromitite samples contain traces (≪1 vol%) of small (< 30 μm) of Ni-Fe-Cu sulphides.

A third microstructural type of chromite, here defined as *non-porous recrystallized chromite* forms the semi-massive and massive chromitite samples of Chernichevo (Fig. 2c–d). This type of chromitite consists of large chromite crystals (grain size ranges between 0.5 and 1 cm) free of pores, displaying triple junctions at 120°. Remarkably, non-porous recrystallized chromite contains higher amounts of sulphides than partly

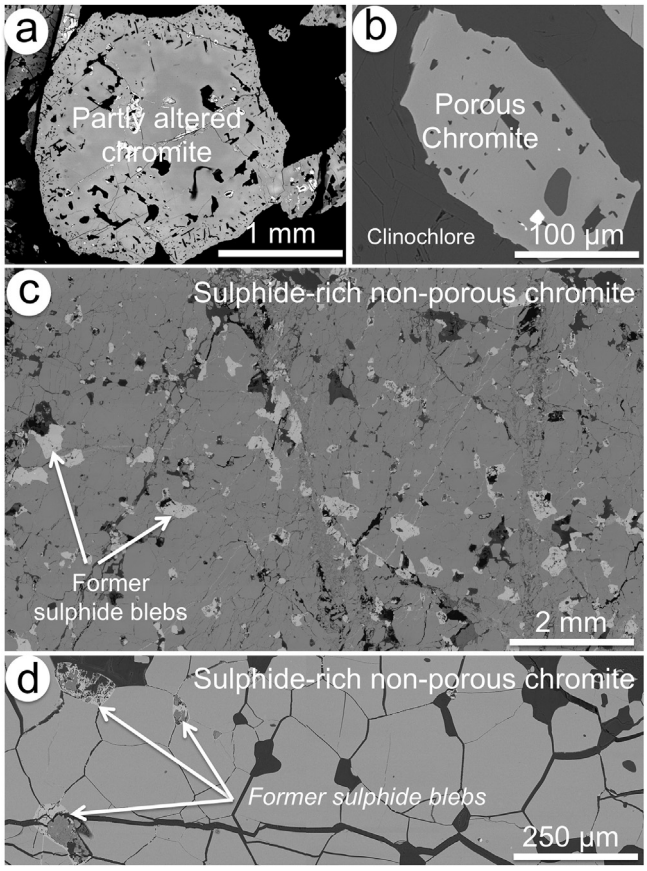

Fig. 2. (a) Back-scattered electron-microscopy microphotographs of representative microstructural types of chromite from Chernichevo chromitites. (a) partly altered chromite of sample CH1-6, (b) porous chromite of sample CH1-9, (c) and (d) non-porous recrystallized chromite from sulphide-rich non-porous chromite (samples CH3-2 and CH2-3 respectively).

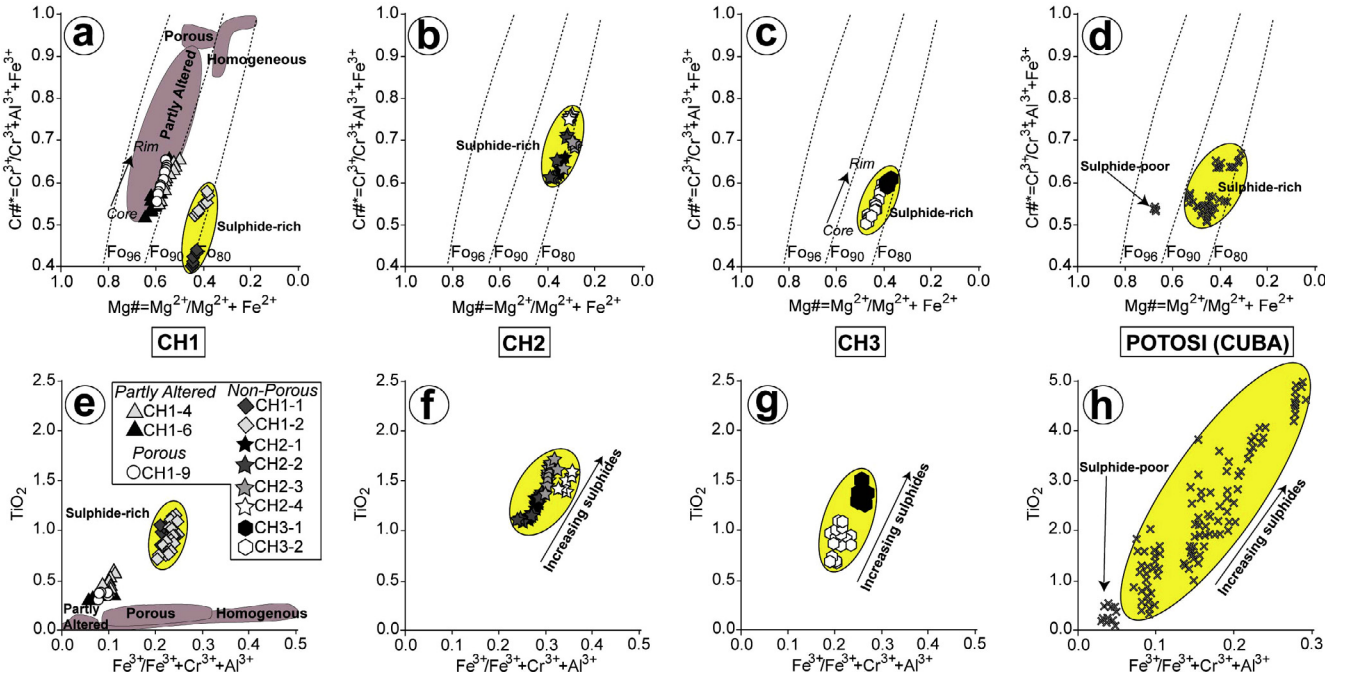

Fig. 3. Plots of the chemistry of chromite (major and minor elements) in terms of Cr# [Cr/Cr + Al + Fe^{3+} atomic ratio] vs Mg# [Mg/Mg + Fe^{2+} atomic ratios (a–c) and TiO_2 vs Fe^{3+}# [$Fe^{3+}/Fe^{3+} + Cr^{3+} + Al^{3+}$ atomic ratio] (e–g). Plots (d) and (h) are shown for comparison and correspond to metasomatized unmetamorphosed chromitites from Potosí in the eastern Cuban ophiolites (Proenza et al., 2001). Purple fields correspond to the compositions of chromite with equivalent microstructural types from the nearby metamorphosed high-Al chromitites of the Golyamo Kamenyane Massif (Gervilla et al., 2012; Colás et al., 2014). Legend is inset in the figure. (For interpretation of the references to color in this figure legend, the reader is referred to the web version of this article.)

altered and porous chromites (up to 5 vol%), which are found as both solid inclusions within and interganular to chromite grains (Fig. 2c–d; Appendix 2). The latter chromites also contain solid inclusions of secondary silicates (i.e. antigorite and minor clinochlore), magnetite, calcite and to lesser extent, apatite and ilmenite, which are found both within and intergranular to chromite grains (Appendix 2). Small masses of Fe-Ni-rich silicates are included in the sulphide inclusions (Appendix 2). No primary olivine was observed in this type of chromitite whereas antigorite is the main constituent of the interstitial matrix.

4.2. Chromite chemistry

Partly altered chromite in semi-massive chromitite have Al-rich cores with Cr# [Cr/(Cr + Al + Fe^{3+}) atomic ratio] = 0.52–0.56, Mg# [Mg/(Mg + Fe^{2+}) atomic ratio] = 0.64–0.58 and $Fe^{3+}/(Fe^{3+} + Al^{3+} + Cr^{3+})$ = 0.06–0.1, surrounded by porous chromite with values of Cr#, Mg# and $Fe^{3+}/(Fe^{3+} + Al^{3+} + Cr^{3+})$ varying from core to rim from 0.58 to 0.65, 0.62 to 0.53 and 0.07 to 0.11, respectively (Fig. 3a; Appendix 3). The composition of porous chromite mostly overlaps with the compositional field of porous rims of partly altered chromite: Cr# = 0.55–0.71, Mg# = 0.59–0.51 and $Fe^{3+}/(Fe^{3+} + Al^{3+} + Cr^{3+})$ = 0.08–0.10 (Fig. 3a; Appendix 3). In contrast, non-porous recrystallized chromite grains are significantly richer in iron in both semi-massive and massive samples (Fig. 3a–c; Appendix 3). Analysis of several chromite grains from different samples produced a chemical trend characterized by an increase in Cr# (from 0.51 to 0.76) and $Fe^{3+}/(Fe^{3+} + Al^{3+} + Cr^{3+})$ (from 0.20 to 0.38), but a decrease in Mg# (from 0.46 to 0.28) (Fig. 3a–c; Appendix 3).

Overall the TiO_2 contents of the Chernichevo chromites are higher (0.31–1.71 wt%) than the reported in other metamorphosed chromite ores from the Eastern Rhodope (Fig. 3e–g; Appendix 3). Interestingly, partly altered and porous chromite fall in a very restricted compositional field [TiO_2 = 0.31–0.6 and $Fe^{3+}/(Fe^{3+} + Al^{3+} + Cr^{3+})$ = 0.06–0.12] whereas non-porous recrystallized chromites show much higher values of TiO_2 (0.67–1.71) and iron ($Fe^{3+}/(Fe^{3+} + Al^{3+} + Cr^{3+})$ = 0.2–0.36), which are positively correlated with the amount of sulphides (Fig. 3e–g; Appendix 3). This compositional trend is distinctively different to that exhibited by other metamorphosed chromites from the nearby Golyamo Kamenyane serpentinite massif, which partly altered and porous chromite overlap with the compositional field of homogeneous (Fe^{3+}-rich) chromite (Fig. 3e). This singularity of the composition in the non-porous recrystallized chromite of Chernichevo ultramafic massif is also observed in the triangular diagram as shown in Fig. 4.

In-situ laser ablation ICP-MS analyses are consistent with the differences noted above (Fig. 5a–h). Thus, partly altered and porous chromites exhibit significantly lower contents of Ti (1691–2966 ppm; average = 2212 ppm; n = 32) compared to non-porous recrystallized chromite (3905–9388 ppm; average = 6838 ppm; n = 65). Higher Ti contents are positively correlated with higher values of Ga, Zn, Mn, and V (Fig. 5a–d; Appendix 4), thus defining two clearly distinct compositional groups that include: (1) partly altered and porous chromite with overall lower Ti, Ga (39–63 ppm; average = 50 ppm), Zn (808–1156 ppm; average = 968 ppm) and V (880–1294 ppm; average = 1102 ppm), and (2) non-porous recrystallized chromite with overall higher contents of Ti and higher Ga (83–199 ppm; average = 138 ppm), Zn (9670–59120 ppm; average = 7598 ppm) and V (1027–1735 ppm; average = 1342 ppm) (Fig. 5a–d; Appendix 4). The positive correlation between Ti and other trace elements is particularly evident in the case of Mn, which defines a clearer positive correlation from the subset of partly altered and porous chromite (1730–2818 ppm; average = 2135 ppm) towards those of non-porous recrystallized chromites with progressively higher amounts of iron and sulphides (2219–4256 ppm, average = 3202 ppm; Fig. 3f and 5c). This contrast with the roughly negative correlation exhibited by Co (39–300 ppm; Fig. 5e; Appendix 4), and the practically constant Ni contents relative to strong variations in Ti exhibited by partly altered and porous chromite (1064–1743 ppm; average = 1315 ppm) and non-porous recrystallized chromite (870–2714 ppm; average = 1393 ppm) (Fig. 5f; Appendix 4). Sc is overall low in all cases (< 9.40 ppm; Appendix 4). The strong differences in the trace element contents of the different

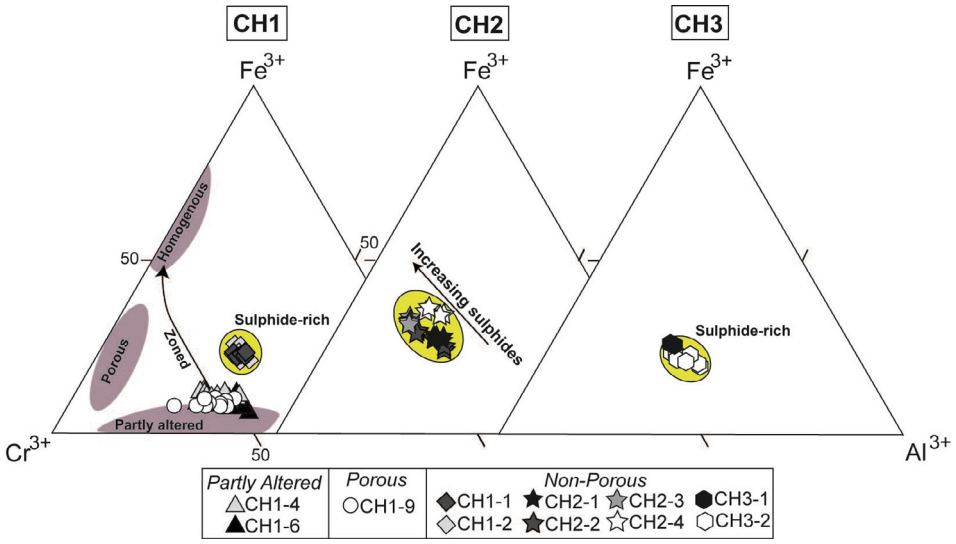

Fig. 4. Variations of Al^{3+}, Cr^{3+} and Fe^{3+} in chromites from the studied chromitites. Compositional fields of metamorphogenetic microstructural types of chromite from the nearby metamorphosed high-Al chromitites of the Golyamo Kamenyane Massif are shown in purple fields (Gervilla et al., 2012; Colás et al., 2014). Legend is inset in the figure.

microstructural types of chromitite is also evidenced by the presence of two different compositional groups in binary plots of Ga *vs.* Zn and Ga + Zn *vs.* V + Mn (Fig. 5g–h).

4.3. Microstructures of the chromitite types

Electron Back-Scattered Diffraction (EBSD) maps were performed on a single grain of partly altered chromite (sample CH1-6; Fig. 6) and selected areas of non-porous recrystallized chromite with progressively higher amounts of Fe_2O_3, TiO_2 and metasomatic sulphides, calcite, apatite and ilmenite (samples CH1-2 → CH2-1 → CH2-3; Figs. 7, 8 and 9).

The partly altered chromite grain of sample CH1-6 displays a band contrast map with no significant changes in the crystallographic orientation between the core and its porous rims (Fig. 6a). The inverse pole figure (IPF) orientation map shows a relatively homogeneous internal distribution of poles in the grain (Fig. 6b), confirming the relatively consistent core-to-rim crystallographic orientation. Small differences in the IPF orientation map are only observed close to silicate and/or late fractures, suggesting that they are due to edge effects and polishing artifacts. Crystallographic continuity between core and rim is also suggested by the distribution of misorientation angles within the grain, indicating that the rim is not randomly oriented with respect to the core (Fig. 6c). Despite the fact that this partly altered grain does not show significant changes in the crystallographic orientation there is a certain degree of distortion accommodated by discrete deformation lamellae as observed in the contrast map (white square in Fig. 6a). Consistently, the misorientation data across this grain reveal maximum misorientation deviation (< 1°) in the zones where these lamellae occur (white square in Fig. 6c). Interestingly, the deformation lamellae display certain curvatures very likely caused by bending and are somehow related with the zones where chromite dominates according to the EBSD phase map (white square in Fig. 6d). Nevertheless, it is worth to note that those domains identified as magnetite in the EBDS map correspond to Fe^{2+}-rich (and Fe^{3+}) chromite as determined by single-spot analyses using EPMA (Fig. 3a and 4); an intermediate phase between chromite and magnetite that is not available in the EBSD database.

The band contrast and IPF orientation maps of three non-porous recrystallized chromite samples reveal the presence of grains with distinct features. The most striking feature is that in those samples with lower amounts of TiO_2, Fe_2O_3 and sulphides (samples CH1-2 and CH2-1) several small faceted grains that form lamellar twins (rectangle A in Fig. 7a and 8b) coexist with larger chromite grains having significant internal crystal bending (rectangles B1 and B2 in Fig. 7b and 8b). The faceted grains typically form high-angle (120°) curved junctions indicative of recrystallization whereas the larger grains with subgrain boundaries exhibit irregular contacts between them and with the smaller faceted grains (Figs. 7 and 8b). The inverse pole figure orientation map indicates no consistent orientation between these two types of grains (Figs. 7 and 8b), which is also observed in the inverse pole figures with different crystal orientation with respect to the specimen XYZ coordinate framework (Figs. 7 and 8c) and the patterns of bulk-crystallographic orientation (CPO) exhibiting various orientation maxima (Figs. 7 and 8d). The distribution of the misorientation angles in a profile across different grains of sample CH1-2 (profile A-A′ in Fig. 7e) is also consistent with different crystallographic orientation of the chromite grains. Small peaks at > 3° misorientation angle in the profile B-B′ correspond to deformation lamellae orientated roughly parallel to the largest length of the crystals (white arrows in Fig. 7e), similar to those described above for the core of the partly altered chromite grain shown in Fig. 6.

On the other hand, the sample with the highest amounts of TiO_2, Fe_2O_3 and sulphides (CH2-3) consists only of small faceted grains with triple joints (Fig. 9a–b). In this sample characterized by a polygonal microstructure, the orientation data obtained from all chromite grains analyzed display near-random to very weak patterns of bulk crystallographic preferred orientation (CPO) with numerous orientation maxima at ⟨1 0 0⟩, ⟨1 1 0⟩, and ⟨1 1 1⟩ (Fig. 9b–d). Here the variation of the misorientation angles in two profiles across different grains (profiles A-A′ and B-B′ in Fig. 9b) is on average significantly much higher (> 15°) than in the other two samples of non-porous recrystallized chromite described above. This is also consistent with our previous observation that chromite grains in this sample exhibit different crystallographic orientation.

4.4. Whole-rock PGE and base-metal contents

The total PGE abundances in the studied chromite ores are mostly between 886 and 3661 ppb (average: 1568 ppb; Appendix 5). The distribution of the PGEs is heterogeneous among the different chromite ores, and even between the different microstructural types. Thus, the sample made up of porous chromite has higher total PGE contents (up to 3661 ppb) than those consisting of partly altered (1770–1942 ppb) and non-porous recrystallized chromites (886–1257 ppb) respectively (Appendix 5). The chromitite samples with porous chromite and those consisting of partly altered chromite have almost identical total IPGE (Os, Ir, Ru) and PPGE (Pt, Pd, Rh) contents, which is reflected in nearly flat patterns in PGE-normalized plots (Fig. 10a). In contrast, non-porous recrystallized chromites exhibit PPGE concentrations that are higher than those of IPGE, producing a positive-slope in the chondrite-

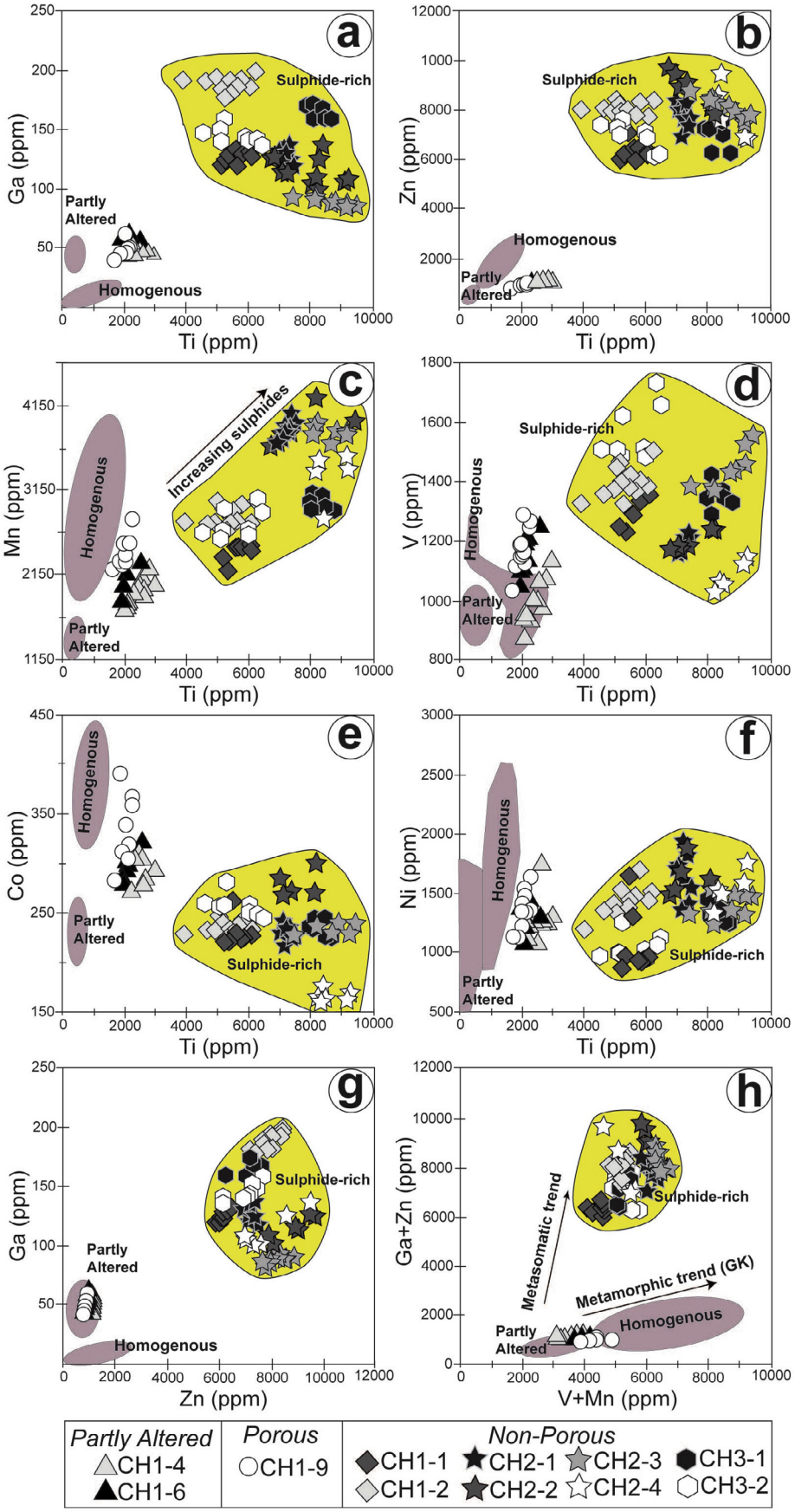

Fig. 5. Compositional variation in terms of Ti vs Ga, Zn, Mn, V, Co and Ni in chromites from the Chernichevo chromitites (data sources are listed in Appendix 4). Composition of chromites from the nearby metamorphosed high-Al chromitites from Golyamo Kamenyane Massif are shown in purple fields (Colás et al., 2014). (For interpretation of the references to color in this figure legend, the reader is referred to the web version of this article.)

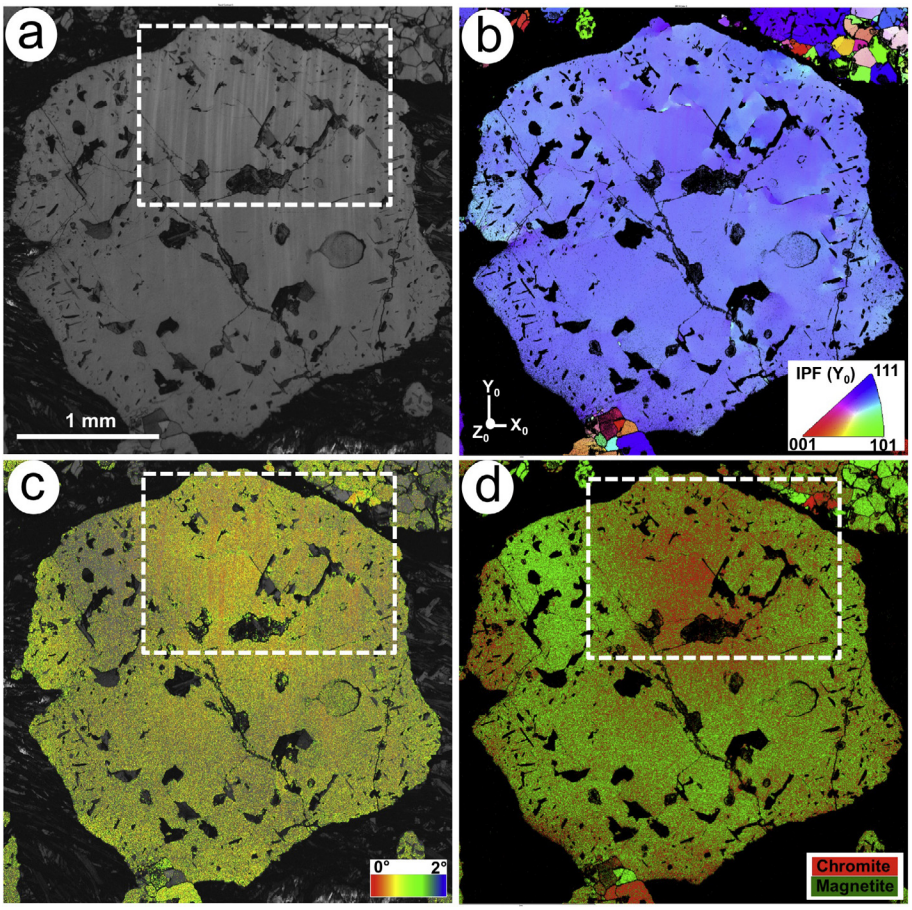

Fig. 6. EBSD and EDS maps of an individual partly altered chromite grain representative of Chernichevo chromitite sample CH1-6. (a) Orientation contrast map showing different gray scale changes in crystallographic orientations with dark areas corresponding to grain boundaries, holes and fractures or undeformed chlorite grains. (b) Inverse pole (IPF) map where colors show different orientations relative to the Y_0 direction. (c) Color coded EBSD map depicting the mean orientation per grain. (d) EDS map of phases. Note that in all maps only chromite and magnetite were indexed and the step size of all maps was 2 μm and a dotted white line rectangle encloses an area with deformation lamellae.

normalized PGE patterns (Fig. 10a). The higher amounts of PPGE in those samples are related to the proportion of sulphides, and particularly those that are Cu-rich. Thus, non-porous recrystallized chromites with the highest proportion of sulphides have overall the highest bulk-rock concentrations of Pt + Pd + Rh and Cu (Appendix 5). Porous chromite also contains the highest amount of gold (up to 50 ppb), which is highly variable within different samples with partly altered (6–16 ppb) or non-porous recrystallized chromite microstructures (4–47 ppb) (Appendix 5).

5. Mineralogy of inclusions in chromitite

5.1. Silicates

Chlorite and antigorite are identified as inclusions or interstitial to chromite in partly altered, porous and non-porous recrystallized chromites, however their composition varies strongly depending on their microstructural position (Appendix 6). Chlorite associated with partly altered and porous chromite in semi-massive chromites (n = 49) varies within the following ranges: Si = 29.47–36.55 wt%, Al = 11.38–20.18 wt%, Mg = 31.34–34.11 wt%, and Fe = 1.48–2.19 wt%; whereas that related to non-porous recrystallized chromite from massive chromitites (n = 24) is enriched in FeO (2.49–3.28 wt%) but lightly depleted in SiO_2 (30.14–34.17 wt%), Al_2O_3 (13.11–19.67 wt%), and MgO (30.94–33.57 wt %) (Appendix 6). The Fe/(Fe + Mg) ratio is < 0.06, overlapping the compositional field of clinochlore as defined by Hey (1954). All analyzed crystals contain significant amounts of Cr_2O_3 (up to 2.69 wt%) and, to lesser extent, NiO (up to 1.93 wt%) (Appendix 6).

Antigorite (n = 39) associated with non-porous recrystallized chromite has variable contents of SiO_2 (37.70–44.07 wt%), MgO (26.17–40.44 wt%) and FeO (1.61–11.98 wt%), and exhibits relatively high amounts of Al_2O_3 (0.11–1.45 wt%), NiO (0.79–1.8 wt%) and Cr_2O_3 (< 0.86 wt%) (Appendix 6).

5.2. Sulphides

Partly altered and porous chromites from semi-massive chromitites contain traces (≪1 vol%) of small-sized (< 30 μm) sulphides of Ni-Fe (pentlandite, millerite, heazlewoodite ± godlevskite) and Fe-Cu (chalcopyrite and bornite). The cores of partly altered chromite host single isolated grains of pentlandite or more frequently composite inclusions of pentlandite-chalcopyrite-bornite ± (millerite), which may contain submicron-sized inclusions of Pd-Bi compounds (Fig. 11a–c). In contrast, the porous rims or the altered silicate matrix contain Ni-rich pentlandite replaced by heazlewoodite and/or magnetite. In the porous chromite, the sulphides are always associated with chlorite filling pores and consist of single or composite grains of all the above listed Ni-Fe-Cu sulphides (Fig. 11d–f). Frequent grains of pentlandite are partly replaced by heazlewoodite and magnetite in both porous chromite and silicate matrix (Fig. 11e–f).

Non-porous recrystallized chromite from massive chromitites contains up to 5 vol% of sulphides as both solid inclusions within, and interganular to, chromite grains (Fig. 11g–l). Their sulphide assemblage is essentially the same as described above for the semi-massive samples, except that they contain pyrrhotite. Sulphide grains included in chromite, far from the edges or crosscutting fractures, are blebs (< 50 μm) consisting of pyrrhotite and pentlandite, with occasionally associated chalcopyrite or bornite (Fig. 11g–h) and a Pt-Pd-Sb compound; few isolated grains of pentlandite were also identified in this microstructural position. Grains connected with late fractures or the interstitial silicate matrix are much larger (up to 1 mm) and characterized by bubble-like or holly-leaf morphology. They consist of pentlandite with

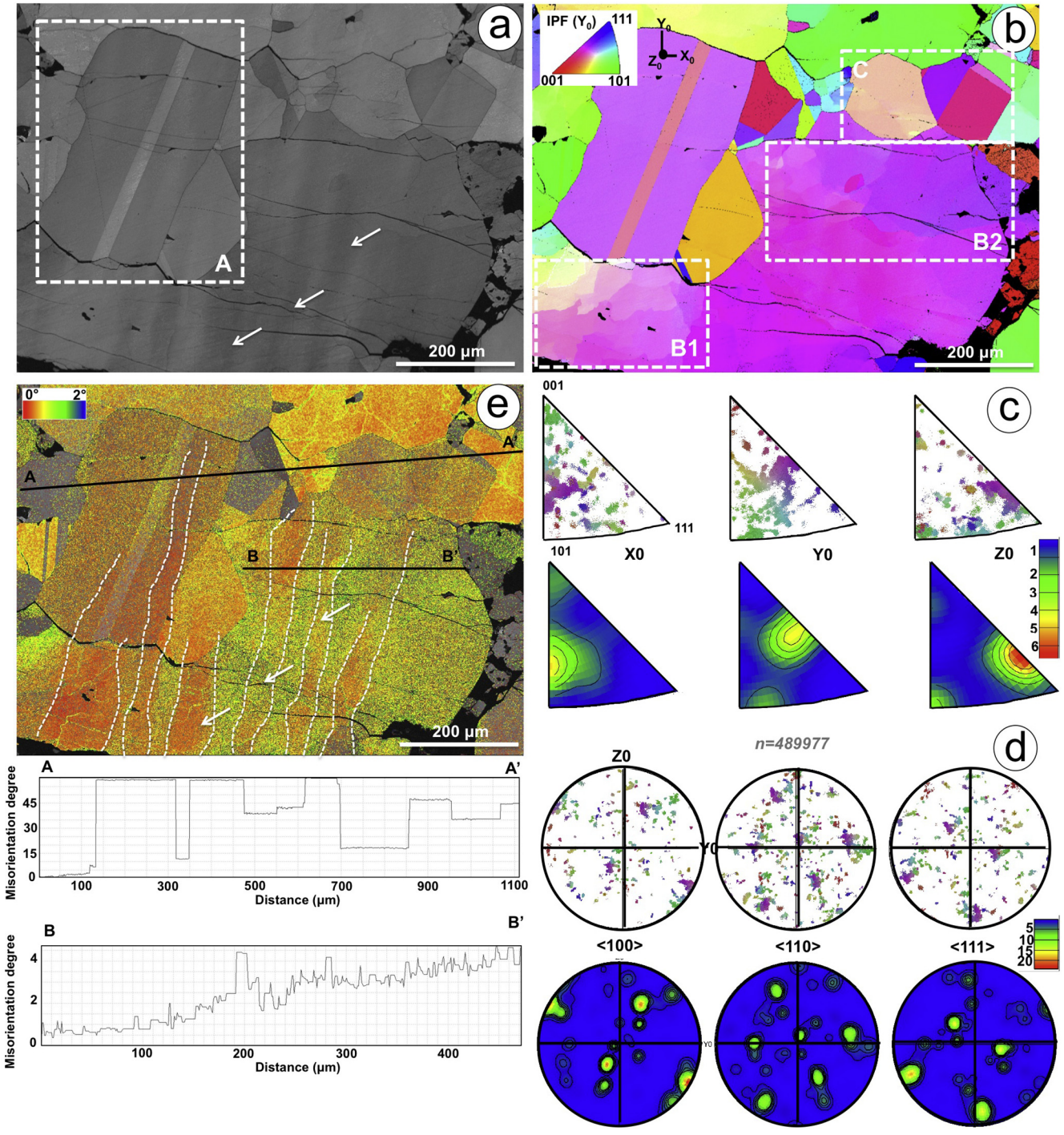

Fig. 7. EBSD maps of the sulphide-poorer non-porous recrystallized chromite of Chernichevo sample CH1-2. (a) Orientation contrast map showing different gray scale changes in crystallographic orientation; the dark areas are grain boundaries, holes and fractures. (b) Inverse pole figure (IPF) maps showing different orientations in colors relative to the Y_0 direction; rectangles B1 and B2 enclose areas with intracrystalline plastic deformation in larger blast, whereas rectangle C enclose an area with smaller strain-free faceted neoblast grains. Distribution of crystallographic preferred orientation (CPO) data of chromite in this area is presented relative to (c) sample coordinates (X, Y, Z) and (d) chromite ⟨1 0 0⟩, ⟨1 1 0⟩ and ⟨1 1 1⟩ pole. Note that data are one point per grain data, smoothed with a Gaussian fit half-width and presented on lower-hemisphere equal-area pole figure. Colors in (c) and (d) are the same as in (b). (e) Misorientation map scaled from 0 to 2° and representative misorientation profiles across the selected area. A dotted white line and arrows indicate areas with maximum misorientation degrees corresponding to deformation lamellae in chromite.

calcite (Fig. 11i–j), ilmenite (Fig. 11k) and/or apatite. Frequently pentlandite is almost completely transformed to magnetite ± (millerite ± heazlewoodite) (e.g., Fig. 11l). Occasionally chalcopyrite is partly transformed to bornite-magnetite and is also found in the interstitial matrix.

Pyrrhotite (n = 12) associated with pentlandite in non-porous recrystallized chromite has low Ni (< 2.71 wt%) and Co (< 0.12 wt%) contents and exhibits relatively high metal/sulphur ratio (0.84–0.95 wt %; Appendix 7). Pentlandite (n = 77) shows a broad compositional variability of Ni (19.74–47.36 wt%) and Fe (14.47–42.71 wt%), and Co

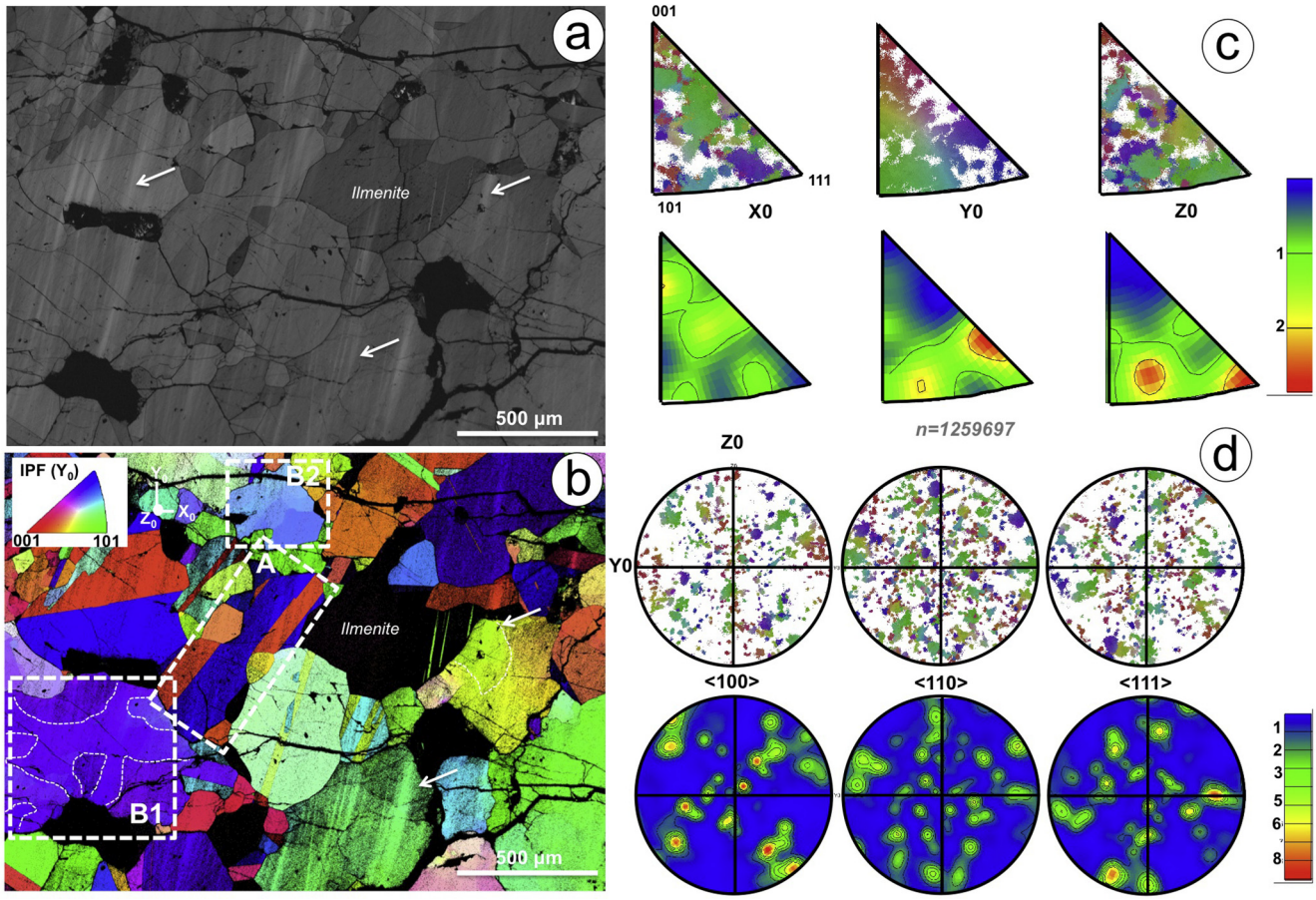

Fig. 8. EBSD maps of the sulphide-richer non-porous recrystallized chromite of Chernichevo sample CH2-1. (a) Orientation contrast map showing different gray scale changes in crystallographic orientation; the dark areas are grain boundaries, holes and fractures. (b) Inverse pole figure (IPF) maps showing different orientations in colors relative to the Y_0direction; rectangle A encloses a larger chromite grain with a deformation twins, whereas rectangles B1 and B2 enclose areas with intracrystalline plastic deformation in larger blast. Distribution of crystallographic preferred orientation (CPO) data of chromite in this area is presented relative to **(c)** sample coordinates (X, Y, Z) and **(d)** chromite ⟨1 0 0⟩, ⟨1 1 0⟩ and ⟨1 1 1⟩ pole. Note that data are one point per grain data, smoothed with a Gaussian fit half-width and presented on lower-hemisphere equal-area pole figure. Colors in (c) and (d) are the same as in (b). White arrows in (a) and (b) indicate areas with maximum misorientation degrees corresponding to deformation lamellae in chromite.

(< 3.88 wt%) (Appendix 7). The composition of pentlandite forming single isolated grains or composite aggregates with pyrrhotite ± chalcopyrite ± bornite in non-porous recrystallized chromites varies within the following ranges: Ni = 22.22–37.93 wt%, Fe = 25.34–37.68 wt%, Co = 0.49–2.8 wt%. In this type of chromite, pentlandite intergrowths with secondary millerite ± heazlewoodite ± magnetite in fractures or in the silicate matrix exhibit similar Ni (28.16–38.95 wt%), Fe (24.47–36.42 wt%), Co (< 2.73 wt%) (Appendix 7). In contrast, pentlandite in partly altered chromites and porous chromite shows overall higher contents of Ni (31.54–47.36 wt%) but lower Fe (14.47–26.63 wt%) and more variable Co (0.29–3.88 wt%) (Appendix 7). The other Ni sulphides (millerite and heazlewoodite) show nearly stoichiometric compositions but contain variable, small amounts of Fe (< 4 wt%) and Co (< 0.31 wt%) (Fig. 12 and Appendix 7). Chalcopyrite and bornite also have very low Ni (< 1.5 wt%) and similar Co (< 0.31 wt%) compared to Ni-rich sulphides (Appendix 7).

5.3. Magnetite

Magnetite grains up to 0.6 mm in diameter were identified associated with Fe-Ni sulphides and included in, and intergranular to, chromite from non-porous recrystallized chromite (Appendix 8). Magnetite (n = 82) forming single isolated grains or composite aggregates with Fe-Ni sulphides having variable but high contents of Cr_2O_3 (up to 4.14 wt%), MgO (up to 2.94 wt%), NiO (up to 1.73 wt%), and TiO_2 (up to 1.26 wt%), low contents of CoO (< 0.40 wt%), MnO (< 0.33 wt%), Al_2O_3 (< 0.20 wt%), and ZnO (< 0.10 wt%), and negligible V_2O_5 (up to 0.06 wt%) (Appendix 8).

5.4. Ilmenite

Ilmenite grains up to 0.5 mm in diameter were identified included in, and intergranular to, chromite from non-porous recrystallized chromite (Fig. 11k; Appendix 2). EPMA analyses of 29 large grains indicate that this type of inclusion contains up to 54.26 wt% of TiO_2 and 9.46 wt% of MgO, as well as variable MnO (0.51–5.91 wt%), V_2O_3 (< 0.6 wt%) and NiO (< 0.10 wt%), corresponding to high contents of the geikielite ($MgTiO_3$) and pyrophanite ($MnTiO_3$) end-members (Appendix 8).

5.5. Carbonates

Carbonates (n = 9) up to 0.5 mm in diameter found as inclusions in non-porous recrystallized chromite show a very constrained composition with high CaO (53.93–56.85 wt%) and traces of FeO

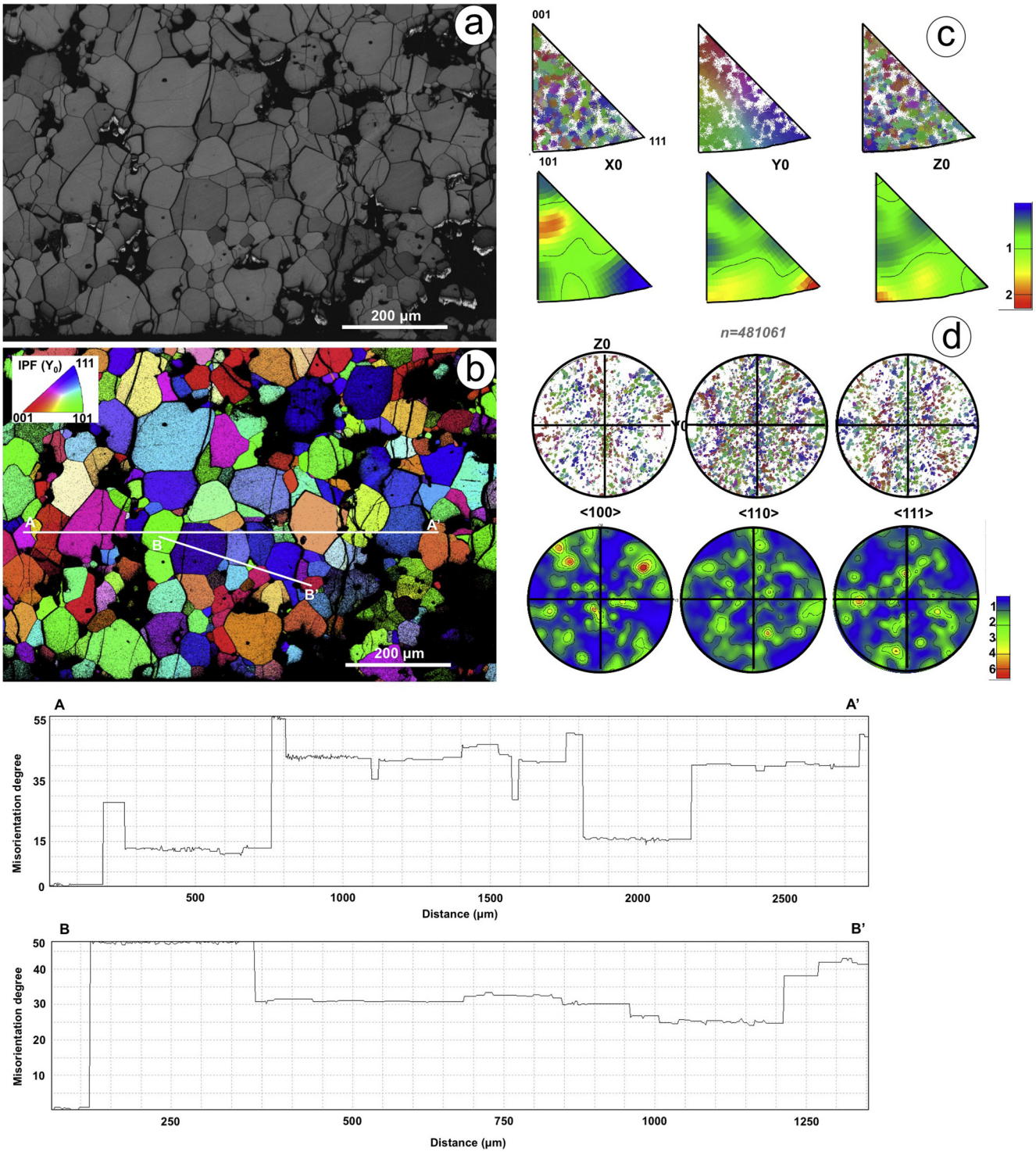

Fig. 9. EBSD maps of the sulphide-richer non-porous recrystallized chromite of Chernichevo sample CH3-2. (a) Orientation contrast map showing different gray scale changes in crystallographic orientation; the w dark areas are grain boundaries, holes and fractures as well as antigorite grains. (b) Inverse pole figure (IPF) map showing different orientations in colors relative to the Y_0 direction; a profile of misorientation (map not shown) also reveal significant differences in orientation among chromite grains of this sample. These different orientation can also be seen in the distribution of crystallographic preferred orientation (CPO) data of chromite relative to (c) sample coordinates (X, Y, Z) and (d) chromite ⟨1 0 0⟩, ⟨1 1 0⟩ and ⟨1 1 1⟩ pole. Note that data are one point per grain data, smoothed with a Gaussian fit half-width and presented on lower-hemisphere equal-area pole figure. Colors in (c) and (d) are the same as in (b).

(0.03–0.36 wt%), Cr_2O_3 (< 0.24 wt%) and MnO (< 0.05 wt%), corresponding to the calcite end-member [Ca/(Ca + Mg + Fe) ratio = 1] (Appendix 9).

5.6. Apatite

Apatite grains (up to 350 µm in diameter) were found as inclusions in non-porous recrystallized chromite grains from a semi-massive chromitite (i.e., CH2-1; Appendix 10). Energy dispersive X-ray spectra

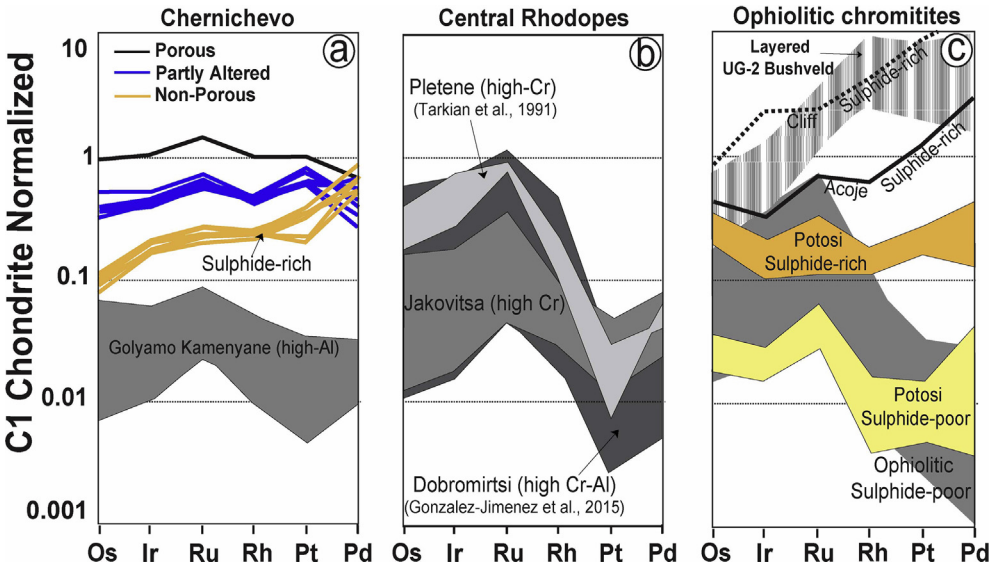

Fig. 10. Bulk-rock PGE compositions of chromitites normalized to C1 chondrite (Naldrett and Duke, 1980). (a) and (b) Chromitites from Chernichevo and other metamorphosed chromitites from the Eastern (Golyamo Kamenyane and Jakovitsa massifs; our unpublished data) and Central Rhodope Metamorphic Complex in Bulgaria (Dobromirtsi and Pletene; Tarkian et al., 1991; González-Jiménez et al., 2015). (c) Examples of sulphide-poor (Proenza et al., 2007 and references herein) and sulphide-rich chromitites (Potosí in eastern Cuba, Acoje in Philippines and Cliff in Scotland; Bacuta et al., 1990; Prichard and Lord, 1993; Proenza et al., 2001) hosted in the mantle section of ophiolites are shown together with those from UG-2 of Bushveld (Naldrett et al., 2012).

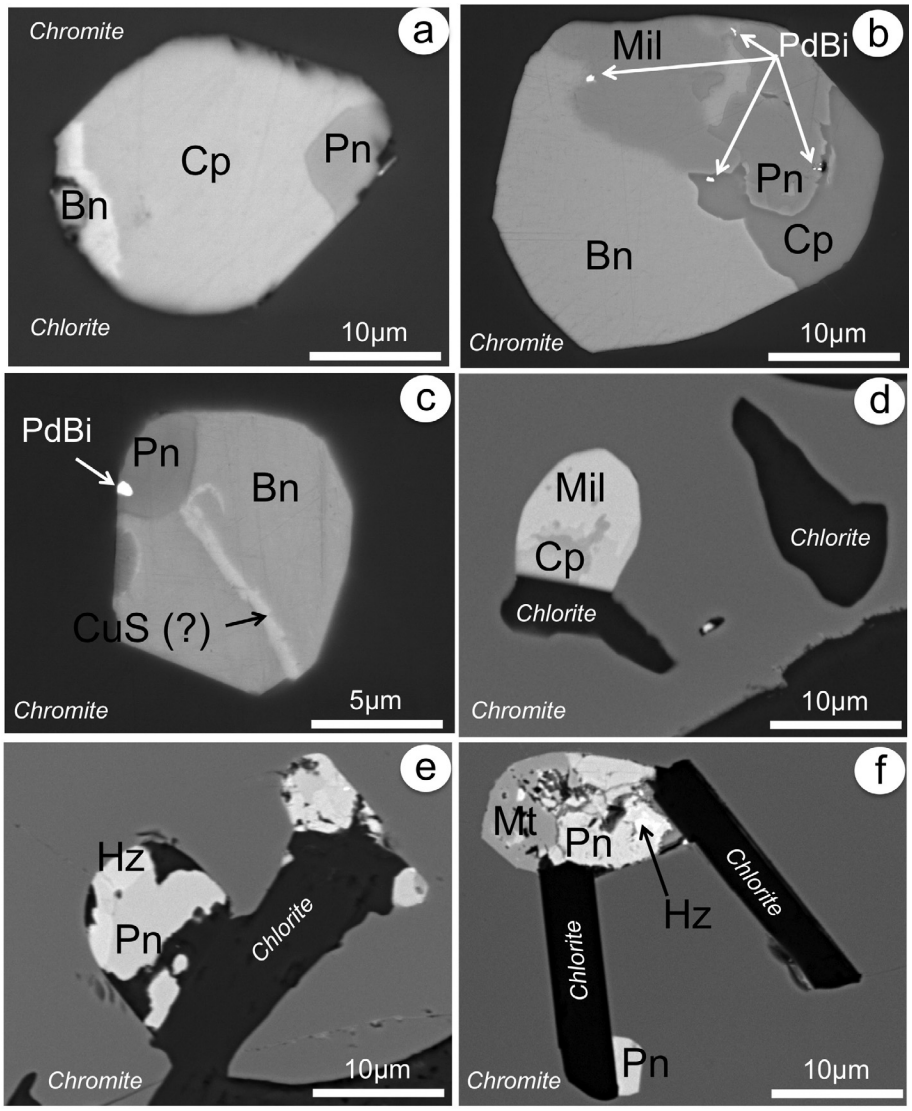

Fig. 11. Backscattered electron images of base-metal sulphides, and associated platinum-group minerals found in chromitites from the Chernichevo ultramafic massif. (a–c) grains included in unaltered chromite cores of partly altered chromite. (d–f) grains included in porous chromite forming rims in partly altered chromite or porous chromite grains. Grains included within (g–h), or interstitial to (i–l) chromites in non-porous recrystallized chromites.

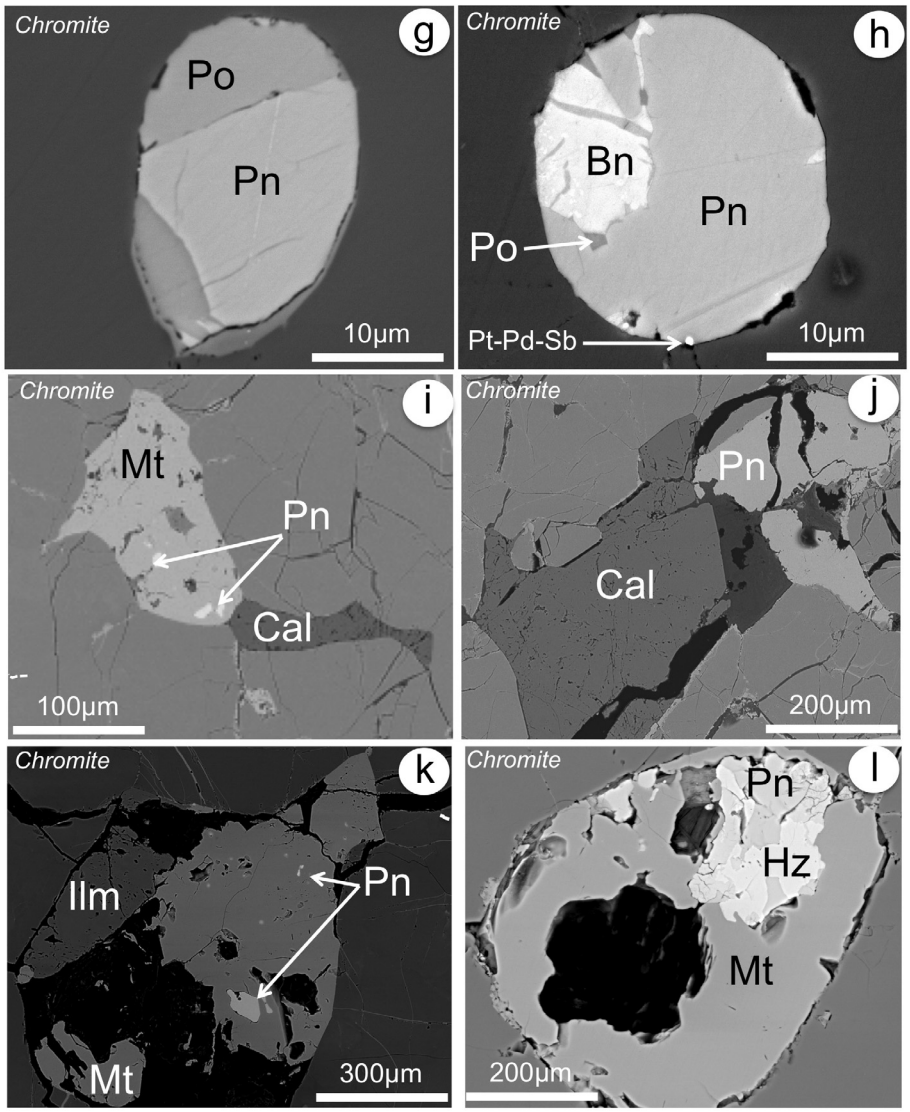

Fig. 11. (*continued*)

(EDS) obtained using an environmental scanning electron microscope (ESEM) indicate that all these grains are Cl-apatite (Appendix 10).

6. Discussion

6.1. Fingerprinting igneous, metasomatic and metamorphic signatures in chromitite

Fig. 3a shows that cores of partly altered chromite should have formed (or equilibrated) in equilibrium with highly magnesian olivine containing ~Fo_{92}. These grains of partly altered chromite also display core-to-rim variation in Cr# and Mg# running between and parallel to the Fo_{90} and Fo_{96} contours. Similar variations in major element composition have been reported in chromitites from the nearby Golyamo Kamenyane serpentinite massif (Fig. 3a; Gervilla et al., 2012; Colás et al., 2014) and metamorphosed ophiolites elsewhere (Barra et al., 2014; González-Jiménez et al., 2016; Colás et al., 2017). These chemical variations are typically produced during the retrograde hydrous metamorphism, when infiltrating fluids derived from the host ultramafic rock promote the reaction of magmatic chromite with the olivine matrix, producing partial to complete replacement of original grains of chromite by secondary Fe^{2+}-rich porous chromite in equilibrium with chlorite (Gervilla et al., 2012). This is a dissolution-precipitation reaction that involves continuous chromite mass loss resulting in the development of porous chromite rims, leaving behind cores that may still preserve the igneous chemical signature (Colás et al., 2017). This is consistent with previous observations (Colás et al., 2014) that cores of partly altered chromite from Chernichevo have a similar distribution of minor and trace elements to those from high-Al chromites from unaltered ophiolites, indicative of crystallization of these chromitites in a spreading center located in the rear of an island arc (i.e., back-arc basin; Zhelyaskova-Panayotova et al., 2000).

In contrast, non-porous recrystallized chromites are significantly richer in FeO than party altered chromites, thus plotting parallel or close to the Fo_{80} contour (Fig. 3a–c). If equilibrium is assumed between chromite and olivine, the progressive increasing of FeO in non-porous recrystallized chromite might reflect the crystallization of their protolith from a melt that had experienced higher rates of fractional crystallization. However, fractional crystallization of silicate melt(s) is relatively rare within single chromitite pods or even between nearby chromitites in the upper mantle section of ophiolite complexes. Rather, it is commonly restricted to layered intrusions (Lord et al., 2006; Mukherjee et al., 2010) or Ural-Alaskan complexes (Garuti et al., 2003; Augé et al., 2005). Moreover, ophiolitic chromitites tend to co-crystallize in equilibrium with ultramagnesian olivine (Fo > 91) and not with an olivine low in magnesium (Fo ~80) as that supposedly must be

in equilibrium with the non-porous recrystallized chromite of Chernichevo (Arai, 1994; González-Jiménez et al., 2014). Therefore, the crystallization of the protolith of non-porous recrystallized chromite from an evolving melt(s) that already precipitated the partly altered chromites must be ruled out.

Compositional variations along the Mg# [Mg/(Mg + Fe^{2+})] axis similar to those observed in Fig. 3a–c have also been attributed to Fe^{2+}→Mg^{2+} exchange between chromite and olivine in chromitites elsewhere. This chemical evolution of chromite is usually associated with diffusion, which affects in greater extent the accessory phase, i.e., accessory chromite in an olivine gangue will become very iron-rich, whereas accessory olivine in a chromitite body will become hypermagnesian (Leblanc and Nicolas, 1992). Thus, lower Mg# should be expected in semi-massive and disseminated chromitites respectively. However, this hypothesis must be also excluded because partly altered and non-porous recrystallized chromite microstructures have been identified in both semi-massive and massive chromitites.. Subsolidus re-equilibration between chromite and olivine during hydrous metamorphism may also produce similar variations of Mg# in chromite (e.g., Barnes and Roeder, 2001; Mukherjee et al., 2010). However, non-porous recrystallized chromite from Chernichevo exhibits distribution of minor and trace elements distinctively different to those described in metamorphosed chromitites from the nearby ultramafic massifs in the Rhodope Metamorphic Complex (Fig. 5a–g; Colás et al., 2014; González-Jiménez et al., 2015) or metamorphosed ophiolites elsewhere (González-Jiménez et al., 2016; McGowan et al., 2015; Colás et al., 2014). Therefore, these geochemical signatures should precede regional metamorphism.

A possible way to explain differences in composition between cores of partly altered and non-porous recrystallized chromites is that they derive from chromitite protoliths that originated in different mantle environments. However, this is not consistent with the fact that these two types of chromite microstructures coexist within a single chromitite body (e.g., CH1; Fig. 3a). It is worth to note that in the non-porous recrystallized chromites the progressive increase in total FeO, Ga, Zn, V, and Mn, and especially, Ti and Fe_2O_3 contents (Figs. 3 and 5) are positively correlated with the amount of sulphides, carbonate, apatite and ilmenite. Mineral assemblages characterized by the coexistence of sulphides, ilmenite, carbonates and phosphates are distinctive feature of metasomatism by volatile-rich alkaline melts that frequently affect peridotites of the subcontinental lithospheric mantle (SCLM) (Gorring and Kay, 2000; Morishita et al., 2008; Hughes et al., 2017), and to a lesser extent from the oceanic mantle (Kogarko et al. 2001; Morishita et al., 2004). Chromitites that have experienced metasomatism by alkaline melts are only known from the SCLM of the Finero massif in Italy (Zaccarini et al., 2004) and the oceanic peridotites of the Potosí Mine in eastern Cuban ophiolites (Proenza et al., 2001). In the latter chromitites, higher iron contents (Fe_2O_3 and FeO) in chromite are also positively correlated with TiO_2, V_2O_3 and MnO, which in turn are also related with the progressively higher abundance of Fe-Ni-Cu sulphides. Proenza et al. (2001) interpreted that higher degrees of interaction with the intruding metasomatic melt had produced chromite ores with higher volumes of sulphides and other metasomatic minerals as well as chromites with progressively higher Fe_2O_3 and TiO_2. Thus, the fact that a given chromite body (i.e., CH1) preserves both partly altered and non-porous recrystallized chromites with variable sulphide contents and rates of chemical modification of chromite has led us to suggest interaction with a single metasomatic melt but at distinctively different melt/rock ratios. This chromitite-melt interaction may have also produced significant recrystallization and coarsening of chromite, explaining why non-porous recrystallized chromites were only found in samples of massive chromitites. These observations allow us to conclude that the increasing of Cr# coupled to decreasing of Mg# was very likely related with metasomatic alteration prior to metamorphism, although a certain degree of modification by metamorphism could not be completely ruled out.

6.2. Sulphide segregation during chromitite-metasomatic melt interaction

As noted above, metasomatism prior to regional metamorphism not only resulted in the modification of the chromite composition but also in the formation of magmatic Ni-Fe-Cu sulphides. Bubble-like contacts of the sulphides with metasomatic apatite, calcite and/or ilmenite suggest mutual immiscibility between sulphide, carbonate and phosphate (Fig. 11i–k; Kogarko et al., 1995 Akizawa et al., 2017; Hughes et al., 2017). The positive correlation between the iron content in the chromite and the higher proportion of sulphides suggests that during the reaction of the chromitite with intruding volatile-rich alkaline melt, chromite must have been strongly enriched in FeO, contributing to a depletion in FeO of the silicate portion of the alkaline melt. This removal of FeO from the alkaline silicate melt may have promoted the achievement of sulphur saturation according to the following reaction proposed by Buchannan and Nolan (1979): $FeO_{(m)} + ½\ S_{2(v)} \Leftrightarrow FeS_{(m)} + ½\ O_{2(v)}$, where m = basaltic melt and v = vapor. Additionally, progressive melt-rock reaction at decreasing melt mass could also promote volatile oversaturation in the upward migrating melt, thus contributing not only to the achievement of sulphur saturation but also in CO_2 and PO_4^{3-} (Pannina and Motorina, 2008; Kamenetsky and Kamenetsky, 2010; Frezzotti and Touret, 2014). This may explain why many sulphides in chromitite bodies from Chernichevo coexist with metasomatic apatite, calcite or ilmenite (Fig. 11i–k).

In the proposed scenario, tiny rounded to droplet-like inclusions of Ni-Fe-Cu sulphides now found inside chromite crystals could represent small volumes of this magmatic sulphide melt(s) that were likely trapped earlier by recrystallizing chromite (Fig. 11g–h). In contrast, larger sulphides with irregular and holly-leaf morphology now found in the interstices between chromite crystals could correspond to remaining volumes of sulphide liquid oversaturated in the carbonate and phosphate component, which was preferentially accumulated in the interstices between larger chromite crystals and silicates (e.g., Fig. 11i). Migration at variable melt/rock ratios and subsequent accumulation of sulphide melts resulted in the formation of the irregular “percolation” front observed in some samples of non-porous recrystallized chromite beyond which only disseminations of small-sized sulphides occur (Appendix 2). The assemblage of pentlandite and chalcopyrite with a few grains of bornite and millerite is also observed in the cores of partly altered chromite, although the proportion and the size of these sulphides are comparatively smaller than in non-porous recrystallized chromite. These observations together with the lack of metasomatic minerals such as apatite or carbonates in these types of chromitites suggest a more limited interaction of the chromitite protolith with the intruding metasomatic melt, which is also consistent with their lower iron and titanium contents (Fig. 3a and e).

The specific temperature at which the aforementioned metasomatic sulphide assemblages were formed can be estimated with some precision, using available experimental data in the Fe-Ni-Cu system. Phase equilibrium relationships (Craig and Kullerud, 1969; Fleet and Pan, 1994; Ballhaus et al., 2001) indicate that once a Fe-Ni-Cu sulphide melt has separated by liquid immiscibility from a basaltic melt, the monosulphide solid solution [$(Fe,Ni)_{1-x}S$; *mss*] is the first solid that crystallizes at ~1000 °C. This leaves a Cu-rich residual melt, which crystallizes to intermediate solid solution (iss) at around 900 °C. So, at this point there is a Ni-rich *mss* portion and a Cu-rich *iss* portion that will experience different subsolidus pathways giving rise to different sulphide assemblages. As the temperature cools to ~610 °C the metal excess in the *mss* is exsolved as pentlandite; this assemblage of *mss* + pentlandite is stable down to 300 °C, below which the Fe-rich *mss* equilibrates to pyrrhotite giving rise to assemblages made up of pyrrhotite + pentlandite similar to those observed in Fig. 11g. Stability fields of phases in the system Fe-Cu-S at atmospheric pressure (Kullerud et al., 1969) show that Cu enrichment in the Fe-Cu-S sulphide melt originally in equilibrium with *mss* will cease once its Cu content reaches ca. 30%, owing to the appearance of intermediate solid solution (*iss*) on

the liquidus. This *iss* phase already formed at ~900 °C is stable down to 300 °C, the temperature at which tie lines predict the coexistence in equilibrium of assemblages of pyrrhotite-bornite similar to those shown in Fig. 11h and chalcopyrite-bornite in Fig. 11a and b (Craig and Scott, 1974 and references therein). Nevertheless, the presence of millerite and bornite in some composite aggregates may also reflect the sub-solidus re-equilibration of the sulphide grains with chromite host, where Fe is removed from the sulphide to fill vacancies in the chromite (Naldrett et al., 1989). Summarizing, the inclusions of pyrrhotite + pentlandite + chalcopyrite (± millerite ± bornite) can be considered crystalline products of sulphide melts enriched in Ni, Fe and Cu, which have experienced a series of polymorphic transformations after the metasomatic reaction with the chromitite and subsequently during peak and post-peak metamorphism (see below).

6.3. Temperature of chromite alteration

In a previous work, Gervilla et al. (2012) analyzed the phase relations in the system Cr_2O_3–MgO–Al_2O_3–SiO_2–H_2O (CrMASH) to estimate the temperature of transformation of the assemblage chromite-olivine to Fe^{2+}-rich chromite-chlorite in chromitites from the nearby Golyamo Kamenyane massif. Considering binary mixing between Cr and Al in the octahedral site of chromite and assuming water-saturated conditions these authors estimated that the formation of Fe^{2+}-rich porous chromite took place at temperatures between ~700 and ~450 °C. Recent refinements of this thermodynamic modeling (González-Jiménez et al. 2015, 2016) now considers all the constituents of the system [i.e., Cr_2O_3–MgO–FeO–Al_2O_3–SiO_2–H_2O (CrMFASH)] as they have also included the binary mixing between Mg^{2+} and Fe^{2+} in the tetrahedral site of chromite. Moreover, Colás et al. (2017) have recently noted that this reaction of alteration involving the dissolution-precipitation of chromite under an open system condition according to SiO_2 (i.e., SiO_2 dissolved in fluids), which would also cause also significant changes in the mineral assemblage of altering chromitite bodies. These latter authors have accounted for the effect of silica by performing P-T-X pseudosections, i.e., P-T diagrams for a fluid saturated CrMFASH system but contoured for SiO_2 wt% and MgO wt%. The results obtained in all these new models indicate that during the formation of Fe^{2+}-rich porous chromite the variations of Cr# at > 0.1 GPa are nearly isobaric and that the gradient of variation of Cr# is strongly dependent on the volumetric chromite/olivine ratio of the rock. This model that is useful to estimate the temperature of formation of Fe^{+2}-rich porous chromite, however has limitations for Fe^{3+}-rich chromite like the non-porous recrystallized chromites because it does not include the mixing properties between ferric iron end-members with inverse spinel structure (i.e., magnetite -Fe_3O_4- and magnesioferrite -$MgFe_2O_4$). We have now refined this model (see details in Appendix 11) considering the Fe_2O_3 in the non-porous recrystallized chromite as a magnetite component, which allows us to carry out a computation using the system Cr_2O_3-FeO-Fe_2O_3-MgO-Al_2O_3-SiO_2-H_2O (CrFMASHO).

Applying our new approach, we have estimated that the transformation of the assemblage chromite + olivine to Fe^{2+}-rich chromite + chlorite took place at 482–432 °C (Appendix 11). This refines the temperatures estimated by Gervilla et al., (2012) for the formation of Fe^{2+}-rich porous chromite in chromitites from the nearby Golyamo Kamenyane massif (~700 and ~450 °C), and overlaps with those obtained for the amphibolite-facies metamorphism of eclogites from the Avren synform (520–440 °C; Mukasa et al. 2003) and other rocks from the Gneiss–Migmatite Complex (570–498 °C; Mposkos et al., 2012). Nevertheless, it is slightly lower than those reported for metasedimentary rocks (650–600 °C; Mposkos and Krohe, 2000, 2006; Mposkos, 2002) of the Kimi Complex (the Greek equivalent of the Avren synform in Bulgaria). From this new modeling it can be also seen that the P-T phase diagrams (Appendix 11) performed for non-porous recrystallized chromite predicts that the assemblage of chromite, olivine and magnetite is stable under the eclogite-facies metamorphism. Although magnetite was not observed in equilibrium with chromite in massive chromitite samples, it is worth to note that EBSD maps of non-porous recrystallized chromite also indexed some of the individual grains of chromite as magnetite, thus attesting the significant magnetite component in them. Moreover, at the temperatures estimated for the formation of Fe^{2+}-rich porous chromite, magmatic chromite is still in equilibrium with magnetite, antigorite and minor brucite in the non-porous recrystallized chromites. It is consistent with our observation that antigorite is the main constituent of the interstitial matrix of non-porous recrystallized chromite, as well as the presence of magnetite within, and intergranular to, chromite grains. It also explains why this type of chromite does not show a porous texture, which requires the dissolution-precipitation of chromite to form a secondary Fe^{2+}-rich chromite in equilibrium with chlorite, as predicted by phase diagrams (Appendix 11).

6.4. Genesis of chromite microstructures

The EBSD maps of chromite show that chromitites from the Chernichevo ultramafic massif exhibit similar deformational features that are disrupted by fractures (Figs. 6, 7, 8 and 9). This indicates that the now-unsupported fragments in the studied samples were originally part of the same grain, suggesting the formation of (sub)-grain boundaries and internal crystallographic bending before fracturing (e.g., Fig. 7b). These observations suggest an initial stage of deformation predominantly in the ductile regime, which was later overprinted by brittle deformation.

The granoblastic microstructure consisting of coarse-grained chromite blasts and finer-grained chromite neoblasts observed in non-porous recrystallized chromites (Figs. 7, 8 and 9) indicates crystal-plastic deformation, which was mainly accommodated by grain-size reduction and recrystallization (Passchier and Trouw, 2005). Similar microstructures of deformation have been reported in other metamorphosed spinel-type oxides (Rosière et al., 2001; Ávila et al., 2015) and chromitites (Ghosh and Konar, 2011; Ghosh et al., 2013, 2014, 2017; Satsukawa et al., 2015). In our samples, plastic deformation may have begun with the onset of intra-crystalline bending now recorded in some large chromite grains preserving subgrain boundaries (grains enclosed within rectangle B1-B2 and C in Figs. 7 and 8b). Progressive deformation of these crystals may have promoted the migration and accumulation of dislocations to discrete zones, giving rise to the formation of subgrain boundaries, and in ultimate instance, grains (rectangles B2 and C in Fig. 7b; Satsukawa et al., 2015; González-Jiménez et al., 2015). Finer strain-free grains in the vicinity of a larger pre-deformed chromite grain show distinct crystallographic affinity (e.g., Figs. 7 and 8c–d), suggesting progressive rotation of a subgrain to form a grain during ongoing deformation. Consistently, small strain-free grains show random, distinctly different orientations to similar adjacent grains and absence of systematic misorientation axes (Figs. 7 and 8c–d). However, this initial stage of high-angle grain boundary formation by subgrain rotation may have been accompanied by grain growth along newly-formed grain boundaries, as is suggested by the lack of substructures in the strain-free idiomorphic grains and their faceted grain boundaries (grains enclosed within rectangle C in Fig. 7b). These observations suggest that grain boundary mobility in the oxide mineral could increase to an extent that grain boundaries sweep through the entire crystal removing the dislocations and subgrain boundaries, thus producing new crystals with near crystallographic continuity (Passchier and Trouw, 2005).

The nearly cubic morphologies shown by some of the newly-formed strain-free grains, and their mutual high angle (120°) triple junction boundaries displaying both daughter and neighbor-daughter dispositions and polygonal habits, indicate that the growth morphology of the boundaries of these new grains was controlled by interfacial energy of the cubic crystals (Halfpenny et al., 2006). The misorientation profiles through these parent and daughter crystals (profiles A-A′ in Fig. 7e and

9b) reveal deviations > 10°, indicating that deformation was still active during crystal growth of these grains. It is also consistent with the occasional presence of feeble substructures and deformation-related lamellar twins within some faceted grains (rectangles A in Fig. 7a and 8b). Moreover, the proposed mechanism of grain boundary migration to produce the strain-free chromite grains is also consistent with the observation that many of the triple junctions exhibited by the fine-grained strain-free grains are frequently joined by secondary chlorite (Fig. 2d). This indicates solute escape from the high-angle migrating front during crystal growth. Thus, the observation that most chromite grains forming non-porous recrystallized chromites are almost inclusion-free suggests that silicates, if originally present in the parent pre-deformed crystal were expelled out to intergranular positions during grain boundary migration (e.g., Satsukawa et al., 2015). These mineral inclusions displaced to interstices among chromite grains acted as cushions that softened the inter-crystalline deformation, thus explaining why we did not observe unsupported fragments at the boundaries between chromite grains. The formation of new small chromite grains (i.e., recovery microstructures), which usually involves the removal of the newly-formed silicates in the most deformed grains, is not only associated with high strain but also requires relatively high temperature conditions (> 700 °C; Christiansen, 1986; Graham et al., 1996; Ghosh and Konar, 2012; Ghosh et al., 2013, 2017; Satsukawa et al., 2015). This is consistent with the fact that mantle rocks of the Kimi Complex in Greece preserve microfabrics suggestive of plastic deformation at temperatures above 765 °C (Mposkos and Krohe, 2006).

On the other hand, EBSD contrast maps reveal the presence of deformation lamellae common to the two microstructural types of chromite grains described above (white arrows in Fig. 7a–e and 8a). This is also highlighted by the existence of distinct plateaus with continuous lattice bending in the misorientation profiles through these grains (profiles A-A′ and B-B′ in Fig. 7e and 9b). Such deformational structures indicate that some additional event of ductile deformation overprinted that of grain-size reduction and recrystallization. This event could be related to: (1) the end of the aforementioned recovery process when the internal strain energy was accommodated by deformation of the entire aggregate, consisting of the two types of chromite crystals; or (2) a different stage of deformation in a discontinuous evolutionary history of the chromitite. We favor the second hypothesis owing to the significant difference in the orientation between the deformation lamellae and other (sub)-structures identified in those grains such as their outlines and deformation twins (squares A in Fig. 7a and 8b). This interpretation becomes clearer when examining the deformation lamellae present in the partly altered chromite grain from the chromitite sample CH1-6 shown in Fig. 6. In this grain, the deformation lamellae cross-cut the entire grain affecting both the core and the rim (white squares in Fig. 6a and c). Single-spot analyses with EPMA and LA-ICP-MS indicates that the igneous signature of chromite is preserved in the core (red zones enclosed in white square of Fig. 6d), whereas the outer Fe^{2+}-richer and Al-poorer porous rim (identified in the EBSD compositional map as magnetite) is metamorphic in origin. If the formation of the porous rim would take place during deformation one could expect asymmetric replacement with formation of subgrain boundaries and crystal bending (e.g., Satsukawa et al., 2015). However, the inverse pole figure (IPF) orientation map of this grain shows core-to-rim crystallographic continuity (Fig. 6b), suggesting that: (1) the core-to-rim structure of the grain predates the formation of the lamellae; (2) the reaction of replacement of magmatic chromite by metamorphic porous chromite took place under static conditions. Static replacement also explains why secondary silicates in these grains are still preserved, unlike those metamorphosed chromites that exhibit chemical re-equilibrium associated with deformation (i.e., recovery microstructures; Satsukawa et al., 2015; Ghosh et al., 2017). This is consistent with some of the mineral reactions preserved in the mafic and ultramafic rocks of the area, which indicate that the hydration of magmatic chromite to form secondary porous chromite and chlorite took place under a static regime between 482 and 432 °C. The observation that a deformation lamella were not identified in non-porous recrystallized chromites of the sample CH2-3 could be related to the deformation produced by local shear zones. Interestingly, active shear-zones have been suggested as a necessary ingredient to produce ductile deformation in chromites from the nearby Golyamo Kamenyane ultramafic massif (Satsukawa et al., 2015).

Summarizing, the microstructures of non-porous recrystallized chromites were produced at a relatively high temperature as a result of crystal-plastic deformation. It involved a first stage with formation and migration of dislocations, subgrain rotation recrystallization, and finally crystal growth by grain boundary migration. In contrast, the microstructure of partly altered chromite originated at much lower temperatures but under static conditions while fluids infiltrated the chromitites. A final event of ductile deformation is recorded by the formation of lamellae in the two microstructural types, which could be related to localised ductile deformation associated with shear zones. This kinematic evolution is in reasonable agreement with that preserved in the ultramafic rocks in the Eastern Rhodope. Mposkos and Krohe (2006) showed that the exhumation of the metaperidotites of the Kimi Complex involved a first stage of plastic deformation under dry conditions at temperatures from above 1000 °C down to ~700 °C, and a subsequent stage of hydration of the rocks under static conditions. The last event of ductile deformation is associated with the development of shear zones during final emplacement of the peridotite slices into the continental crust.

It is worth to note that all the microstructural features observed in non-porous recrystallized chromite are typical for deformation in dislocation-creep regimes (Urai et al., 1986; Passchier and Trouw, 2005), and these include: (1) intra-crystalline deformation defined by subgrain boundaries; (2) dynamic recrystallization of chromite by subgrain rotation; and (3) growth by grain boundary migration recrystallization. This indicates that deformation at high-temperatures in chromite is mainly accommodated by dislocation creep not by diffusion creep, as recently observed in metamorphosed chromitites from the nearby ultramafic body of Golyamo Kamenyane (Satsukawa et al., 2015) and the Neoarchean Sittampundi Complex of southern India (Ghosh et al., 2017). Noteworthy, chromitites from Cherenichevo that contain progressively higher amounts of Ti and overall iron (as well as metasomatic minerals) show the highest degrees of grain reduction and recrystallization in EBSD maps, i.e., CH1-2 → CH2-1 → CH3-2 (Figs. 3, 7, 8, and 9). This suggests that the aforementioned mechanism of accommodation of deformation seems to be more effective in those chromitites modified to a higher degree by the metasomatic alkaline melt prior to metamorphism. This observation is contrary to previous ones from the literature, where deformation controlled the effectiveness of the local chemical re-equilibration of chromite (e.g., Satsukawa et al., 2015; Ghosh et al., 2017). Indeed, the higher amounts of TiO_2 and Fe_2O_3 (i.e., ulvospinel and magnetite components) in chromite from Chernichevo aided to intra-crystalline deformation of chromites. This discrepancy highlighted by our observations illustrates the necessity for additional experiments to determine the role of composition on deformation mechanisms of chromite. Interestingly, Kruse and Stünitz (1999) observed a similar relationship between microstructure and chemistry for hornblende from mylonites of anorthositic to gabbroic rocks. They showed that the compositional difference between porphyroclasts and recrystallized hornblende grains is not due to diffusional exchange after recrystallization, but more probably to heterogeneous nucleation and growth of compositionally different hornblende.

6.5. Metamorphism of magmatic sulphides

As noted above, chromitites from Chernichevo have experienced UHP metamorphism (> 2.5 GPa) with peak temperatures > 1200 °C. These conditions are far beyond the stability limits of sulphides raising

the possibility of partial melting of the magmatic sulphides in chromite and therefore the formation of metamorphic (anatectic) sulphide melt (s). Partial melting of sulphide assemblages containing Ni, Fe and Cu would result in the initial separation of a Cu-rich liquid owing to the lower melting point of Cu-sulphides (Bockrath et al., 2004; Peregoedova et al., 2004). Once formed, this Cu-rich liquid would be rapidly removed from the remaining (Ni-Fe)-rich solid and probably extracted out from the chromitite, unless we consider a closed system. Re-melting of magmatic sulphides in a closed system could explain the rounded to droplet-like morphology of many composite aggregates consisting of Ni-Fe-Cu sulphides found inside chromites forming the cores of partly altered chromites and non-porous recrystallized chromite microstructures (e.g., Fig. 11g–h). However, this hypothesis is difficult to reconcile with the EBSD data indicating crystal-plastic deformation in solid state instead of partial melting of chromite. Indeed, substantial high temperature could favor Fe diffusion between sulphides and larger chromite host crystals, explaining the relative abundance of bornite, millerite, and some isolated Ni-rich pentlandite grains in these microstructural positions.

On the other hand, many composite grains are found intergranular in non-porous recrystallized chromite or associated with chlorite, filling pores of porous chromite consist of pentlandite coexisting with, or replaced by, heazlewoodite ± millerite ± magnetite (Fig. 11e–f and l). Whereas nothing can be concluded about the primary or secondary origin of some of these pentlandite grains, their replacement by more Ni-rich and S-poor sulphides associated with secondary chlorite or other unknown Ni-rich silicates suggests a link with metamorphism (Eckstrand, 1975; Frost, 1985; Klein and Bach, 2009). Phase relations in the Ni-Fe-O-S system indicate that assemblages comprising heazlewoodite ± millerite ± magnetite can coexist with, or be formed after, pentlandite under the very low fO_2-fS_2 conditions that usually prevail during the initial stages of serpentinization at ~400 °C (Craig, 1973; Klein and Bach, 2009; Gole, 2014; Debret et al., 2017). Indeed, the slightly higher temperatures estimated for the Fe^{2+}-rich porous chromite (482–432 °C) suggest that liberation of pervasive fluids lowering fO_2 and fS_2 took place once the reaction of chromite alteration progressed. In this scenario, the hydration of olivine from the interstitial chromitite matrix (or host peridotite) could also have transformed to chlorite (predominantly in samples of partly altered and porous chromite) and antigorite (predominantly in samples of non-porous-recrystallized chromites) while releasing some H_2 (Bach et al., 2006). This hydrogen could combine with ½ O_2 to form H_2O and/or with S to form H_2S, lowering fO_2 and fS_2. Under these conditions, pentlandite grains originally located at the edge of chromite crystals or within the interstitial silicate matrix reacted with H_2 and/or H_2O breaking down to heazlewoodite and magnetite, according to the two following idealized reactions (Klein and Bach, 2009; Sciortino, 2014):

$$Ni_{4.5}Fe_{4.5}S_8 + H_2O \rightarrow 1.5Ni_3S_2 + 1.5Fe_3O_4 + H_{2,aq} + 5H_2S_{,aq}$$

$$2Fe_{4.5}Ni_{4.5}S_8 + 12H_2O + 4H_2 \rightarrow 3Ni_3S_2 + 3Fe_3O_4 + 16H_2S$$

The copious amount of H_2S released to the circulating fluids during this reaction and concomitant silicate serpentinization may still react with the previously formed heazlewoodite (Ni_3S_2) loosing its S, forming secondary millerite (NiS) (Klein and Bach, 2009):

$$Ni_3S_2 + H_2S_{,aq} \rightarrow H_{2,aq} + 3NiS$$

Direct evidence for the reactions (1), (2) and (3) in Chernichevo chromitites are provided by the frequent composite aggregates made up of pentlandite + heazlewoodite + magnetite (Fig. 11f and l), pentlandite + millerite + magnetite as well as relicts of incompletely dissolved pentlandite in magnetite (Fig. 11i and k). Assemblages of godlevskite-heazlewoodite may be also explained as a result of partial re-equilibration of pentlandite grains at ~400 °C (Klein and Bach, 2009) and low fO_2-fS_2 conditions prevailing during the transformation of magmatic chromite to porous chromite. Furthermore, admixing of Fe from pentlandite by re-equilibration with host chromite could also explain the formation of isolated grains of godlevskite in agreement with the tie-lines α-$Ni_{7\pm x}S_6$-pentlandite on the Ni-S phase diagrams of Ueno et al. (2000).

Additionally, the water in the system may also react with remaining pyrrhotite (FeS) to form additional amounts of magnetite and H_2, which also overall contributed to the reducing environment of the process (Debret et al. 2017):

$$2FeS + 11H_2O \rightarrow 2SO_4^{=} + Fe_2O_3 + H_{2,aq}$$

Given that liberation of H_2 to the system remains effective up to olivine consumption (Frost, 1985; Klein and Bach, 2009), slightly higher oxidizing conditions may have promoted the subsequent desulphurization of pyrrhotite-chalcopyrite assemblages to secondary bornite and magnetite in the interstitial matrix of non-porous recrystallized chromites, according to the following equation (Maier and Barnes, 1996):

$$5CuFeS_2 + 5FeS + 6H_2O + 8O_2 \rightarrow Cu_5FeS_4 + 3Fe_3O_4 + 6H_2S_{,aq} + 5SO_{2,aq}$$

The alteration process outlined above implies a change of the magmatic sulphide assemblage from pyrrhotite ± pentlandite ± chalcopyrite ± millerite ± bornite to assemblages containing predominantly Ni-rich sulphides, including pentlandite ± heazlewoodite ± millerite ± magnetite or heazlewoodite ± godlevskite. Overall this process implies leaching of Cu, which is consistent with the variable bulk-rock Cu/Ni + Co ratios in the studied rocks (Appendix 5). Thus, the lower Cu/Ni + Co ratios in bulk-rock samples of porous chromite and partly altered chromite relative to non-porous recrystallized chromite (Appendix 5) suggests that the impact of the proposed alteration was greatest on the rocks with a lower proportion of sulphides. This has a profound impact on the distribution of PGE (see below).

6.6. PGE concentration and remobilization

The total PGE abundances in the Chernichevo chromitites are out of the range reported for typical sulphide-poor mantle-hosted podiform-type chromitites from the upper mantle section of ophiolites from the Bulgarian Rhodopes and elsewhere (Fig. 10a–b). Rather their overall high PGE contents and chondrite-normalized patterns resemble those ophiolitic chromitites rich in Ni-Fe-Cu sulphides of the podiform-type reported from the Potosi Mine in the eastern Cuban and the banded-type from the ophiolites of Acoje in Philippines and Cliff in Scotland (Fig. 10c). These observations together with the fact that PGE and Ni + Co + Cu are positively correlated (Appendix 5) led us to suggest the important role that metasomatic sulphides had for the concentration of PGE in the Chernichevo chromitites. This interpretation is also consistent with the available experimental and empirical data indicating that high concentration of PGE in mantle-hosted chromitites is mainly related to the formation of sulphide minerals (O'Driscoll and González-Jiménez 2016). The close link between PGEs and base-metal sulphides in the Chernichevo chromitite may reflect the preferential partitioning of the PGE towards the immiscible Ni-Fe-Cu sulphide melt that was segregated from the metasomatic alkaline melt, owing to their extremely high $D^{\text{sulfide melt/silicate melt}}$ (Mungall et al., 2005). Experimental data indicate that during the fractional crystallization of these types of PGE-bearing sulphide melts, IPGEs (Ir, Os and Ru) and rhodium partition into the early-formed *mss* whereas Pt and Pd, partition into the Cu-rich residual liquid formed after *mss* crystallisation, and finally in their crystalline product (Li et al., 1996; Ballhaus et al., 2001; Bockrath et al., 2004). This phenomenon is, however, dependent on the presence and concentration of semi-metals within the Cu-rich sulphide liquid, since their presence may cause the formation of platinum group minerals (PGM) of these elements around the margins of sulfide grains

(Peregoedova et al., 2004; Piña et al., 2012). In Chernichevo the highest amounts of PPGE in the chromitite closely correlate with the highest amount of sulphides, and particularly Cu-rich sulphides (Fig. 10a and Appendix 5). These observations indicate that fractionation of Pt and Pd was mainly controlled by Cu-rich sulphides, consistent with the fact that only two tiny compounds of PdBi (Fig. 11b–c) and one Pt-Pd-Sb (Fig. 11h) were found at the margin of larger Ni-Fe-Cu sulphides. Interestingly, chromitites containing sulphide ores characterized by high Cu/Ni ratios, either hosted in the mantle or the crust, also display positive-sloped PGE-normalized patterns similar to those we have described here for non-porous recrystallized chromites (Fig. 10c).

However, we have noted above that hydrous metamorphism of the Cherenichevo chromitites has transformed the magmatic Ni-Fe-Cu sulphides to secondary Ni-rich and S-poor sulphides. The intensity of this alteration was greater in the protoliths of porous chromite and partly altered chromite. In these chromitites with the lower proportion of sulphides, the metamorphic modification of the original magmatic sulphide assemblage not only implied major leaching of Cu (and minor Fe) but also of PPGE. This is also evidenced by their much lower bulk-rock Cu contents and similar to slightly lower PPGE concentrations relative to IPGE than non-porous recrystallized chromites (Fig. 10a and Appendix 5). Previous studies based on theoretical estimates, and experimental and empirical data indicate that Pt and Pd can be transported as bisulphide, chloride and/or hydroxide complexes by a neutral to alkaline fluid generated at the T-fO_2-fS_2 conditions in which porous chromite were formed in Chernichevo (e.g., Mountain and Wood, 1988; Thalhammer et al., 1990; Barnes and Liu, 2012). It has also been proposed that transport of Pt and Pd in these types of hydrothermal fluids can be also accompanied by metals such as Cu. Therefore, the influence of hydrous metamorphism on the PGE distribution in the Chernichevo chromitites is thus regarded as a general leaching processes, which led to the impoverishment in the most mobile PGE together with Cu. If this is true, one could speculate that these chromitites originally had much higher PPGE. Assuming that IPGE were immobile during metamorphism, we can use them as a proxy to estimate the original PPGE contents in the porous and partly altered chromite. Thus, a simple exercise of comparison with sulphide-rich chromitites having identical IPGE contents and Ni/Cu ratios of the sulphide mineralization led us to speculate that these chromitites could have had prior to metamorphism Pt and Pd contents of at least 10 times the chondritic values. If so, the relatively smaller fractions of tiny sulphides now found in porous and partly altered chromites would be much strongly enriched in PGE than the volumetrically higher Ni-Fe-Cu mineralization associated with non-porous recrystallized chromite. This observation illustrates that a high concentration of PGE in sulphide liquids is possible without the necessity to interact with large volumes of silicate magma as usually reported for conventional Ni-Fe-Cu deposits. This situation that is rather common in xenoliths that have sampled the SCLM (e.g., Hughes et al., 2017) and has also been reported in the Platinova Reef from the Skaergaard Intrusion in east Greenland by Holwell et al. (2015). In this ore deposit, the authors reported that very small volumes of tiny Ni-Fe-Cu sulfides were also able to acquire extremely high PGE tenors despite high R factors (i.e., mass of silicate magma/sulphide magma; Campbell and Naldrett, 1979). These observations together with ours illustrate the complexity of magmatic processes in the mantle as regards to forming PGE-rich sulphide mineralization.

7. Conclusions

Chromitites hosted in the mantle section of the metamorphosed ophiolite from Chernichevo in southern Bulgaria record a complex post-magmatic history. A first stage is related with the modification of the chromitite, very likely in the mantle, by reaction with intruding volatile-rich alkaline melt at variable melt/rock ratios. This resulted in a substantial modification of the composition and microstructure of the magmatic chromite while depositing a suite of metasomatic minerals, including sulphides, ilmenite, apatite and calcite. The formation of these metasomatic minerals is related to a mechanism of sulphide-phosphate-carbonate immiscibility interpreted as the consequence of chemical interaction between intruding melt and the host chromite. In this scenario, the variable extent of the chromitite-melt interaction has promoted the segregation of different amounts of immiscible sulphide liquid, which accounted for the concentration of abnormally, but variably, high tenors of the platinum-group elements in these chromitites. A second post-magmatic stage of alteration of the chromitite is related to regional metamorphism, although its affects vary widely, depending on the composition produced after the alkaline metasomatism. Chromitites with very low amounts of sulphides and lower degrees of chemical modification of chromite were substantially affected by hydrous metamorphism. Thermodynamic modeling shows that this alteration resulted in the formation of secondary Fe^{+2}-rich porous chromite in equilibrium with chlorite, giving rise to partly altered and porous chromite. This alteration processes took place at 482–432 °C and under static conditions within the P-T conditions of amphibolite-facies metamorphism. In contrast, chromitites with the highest degree of metasomatic modification (i.e., higher iron content and abundance of metasomatic minerals) were not substantially affected by hydrous metamorphism, apart from the serpentinization of the silicate matrix of the chromitites. In this type, the strongest effects of metamorphism were limited to plastic deformation of the chromite grains giving rise to non-porous recrystallized chromite microstructures; these originated at temperatures higher than those reported for the hydrous metamorphism (> 700 °C). Water-saturated and highly reducing conditions prevailing during hydrous metamorphism resulted in the transformation of the magmatic Ni-Fe-Cu sulphides to a new generation of Ni-rich and S-poorer sulphides. This change of the mineral assemblage is recorded by an increase in Ni and a loss of Cu tenors in the whole rock, which is coupled with a decrease in Pt and Pd. This is an evidence that a removal of Cu sulphides during hydrous metamorphism is an effective way to mobilize PGE.

Acknowledgements

Funding for this research was provided by the project CGL2014-55949-R granted by the Spanish “Ministerio de Economía y Competitividad”. Additional funding was provided by the Ramón y Cajal Fellowship RYC-2015-17596 granted by the Spanish MINECO to JMGJ. Jesús Montes is acknowledged for preparation of thin sections. Isabel Sáncez Almazo and Alicia González Segura (Centro de Instrumentación Científica of the University of Granada), Augusto A. Rodríguez Díaz (Instituto de Geofísica, UNAM) and Carlos Ortega-Obregón (Centro de Geociencias, UNAM) for their assistance with HRSEM ESEM and LA-ICP-MS, respectively.

Appendix A. Supplementary data

Supplementary data associated with this article can be found, in the online version, at https://doi.org/10.1016/j.oregeorev.2018.07.024.

References

Akizawa, N., Miyake, A., Ishikawa, A., Tamura, A., Terada, Y., Uesigi, K., Takeuchi, A., Arai, S., Tanaka, C., Igami, Y., Suzuki, K., Kogiso, T., 2017. Metasomatic PGE mobilization by carbonatitic melt in the mantle: evidence from sub-μm-scale sulphide-carbonaceous glass inclusions in Tahitian harzburgite xenolith. Chem. Geol. 475, 87–104.

Arai, S., 1994. Compositional variations of olivine-chromian spinel in Mg-rich magmas a guide to their residual spinel peridotites. J. Volcanol. Geotherm. Res. 59, 273–293.

Augé, T., Genna, A., Legendre, O., 2005. Primary platinum group mineralization in the Nizhny Tagil and Kachkanar ultramafic complexes, Urals, Russia: a genetic model for PGE concentration in chromite-rich zones. Econ. Geol. 100, 707–732.

Ávila, C., Lagoeiro, L.E., Ferreira-Barbosa, P., Graça, L., 2015. EBSD analysis of rhombohedral twinning in hematite crystals of naturally deformed iron formations. J. Appl. Cryst. 48, 212–219. https://doi.org/10.1107/S1600576714025928.

Bach, W., Paulick, H., Garrido, C.J., Ildefonse, B., Meurer, W.P., Humphris, S.E., 2006.

Unraveling the sequence of serpentinitzation reactions: petrography, mineral chemistry, and petrophyscis of serpentinites from MAR 158N (ODP Leg 209, Site 1274). Geophys. Res. Lett. 33https://doi.org/10.1029/2006GL025681. L13306.
Bacuta, G.C., Kay, R.W., Gibbs, A.K., Lipin, B.R., 1990. Platinum-group element abundance and distribution in chromite deposits of Acoje block, Zambale ophiolite complex, Philippines. J. Geochem. Explor. 37, 113–145.
Ballhaus, C., Tredoux, M., Späth, A., 2001. Phase relations in the Fe-Ni-Cu-PGE-S system at magmatic temperature and application to massive sulfide ores of the Sudbury Igneous Complex. J. Petrol. 42, 1991–1996.
Barnes, S., Liu, W., 2012. Pt and Pd mobility in hydrothermal fluids: evidence from komatiites and from thermodynamic modelling. Ore. Geol. Rev. 44. https://doi.org/10.1016/j.oregeorev.2011.08.004.
Barnes, S., Roeder, P.L., 2001. The range of spinel compositions in terrestrial mafic and ultramafic rocks. J. Petrol. 42, 2279–2302.
Barra, F., Gervilla, F., Hernández, E., Reich, M., Padrón-Navarta, J.A., 2014. Alteration patterns of chromian spinels from La Cabaña peridotite, south-central Chile. Mineral. Petrol. 108 (6), 819–836.
Bockrath, C., Ballhaus, C., Holzheid, A., 2004. Fractionation of the platinum-group elements during mantle melting. Science 305, 1951–1953.
Bonev, N., 2006. Cenozoic tectonic evolution of the Eastern Rhodope massif (Bulgaria): basement structure and kinematics of syn- to post-collisional extensional deformation. In: Dilek, Y., Pauides, S. (Eds.), Mediterranean Region and Asia. Geol. Soc. Am. Spec. Paper, pp. 211–235.
Bonev, N., Moritz, R., Márton, I., Chiaradia, M., Marchev, P., 2010. Geochemistry, tectonics, and crustal evolution of basement rocks in the Eastern Rhodope Massif, Bulgaria. Int. Geol. Rev. 52 (2–3), 269–297.
Buchannan, D.L., Nolan, J., 1979. Solubility of sulphur and sulphide immiscibility in synthetic tholeiitic melts and their relevance to Bushveld complex rocks. Can. Mineral. 17, 483–494.
Burg, J.-P., Ricou, L.-E., Ivanov, Z., Godfriaux, I., Dimov, D., Klain, L., 1996. Syn-metamorphic nappe complex in the Rhodope Massif.Structure and kinematics. Terra Nova 8, 6–15.
Campbell, I.H., Naldrett, A.J., 1979. The influence of silicate:sulfide ratios on the geochemistry of magmatic sulfides. Econ. Geol. 74, 1503–1506. https://doi.org/10.2113/gsecongeo.74.6.1503.
Christiansen, F.G., 1986. Deformation of chromite: S.E.M. investigations. Tectonophysics 121, 175–196.
Colás, V., González-Jiménez, J.M., Griffin, W.L., Fanlo, I., Gervilla, F., O'Reilly, S.Y., Pearson, N.J., Kerestedjian, T., Proenza, J.A., 2014. Fingerprints of metamorphism in chromite:new insights from minor and trace elements. Chem. Geol. 389, 137–152.
Colás, V., Padrón-Navarta, J.A., González-Jiménez, J.M., Fanlo, I., Sánchez-Vizcaíno, V., Gervilla, F., Castroviejo, R., 2017. The role of silica in the hydrous metamorphism of chromite. Ore Geol. Rev. 90, 274–286.
Collings, D.A.T., 2014. The tectono-metamorphic evolution of the Rhodope Massif, Bulgaria (Ph.D). University of Leeds, Bulgaria, pp. 204.
Craig, J.R., Kullerud, G., 1969. Phase relations in the Cu-Fe-Ni-S system and their application to magmatic ore deposits. Econ. Geol. 4, 344–358.
Craig, J.R., Scott, S.D., 1974. Sulfide phase equilibria. In: Ribbe, P.H. (Ed.), Sulfide Mineralogy Rev. Mineral. Geochem. 1, CS-l-CS-1 10.
Craig, J.R., 1973. Pyrite-pentlandite assemblages and other low temperature relations in the Fe-Ni-S system. Am. J. Sci. Cooper 273-A, 496–510.
Debret, B., Andreani, M., Delacour, A., Ruméjon, S., Trcera, N., EIMF, Williams, H., 2017. Assessing sulfur redox state and distribution in abyssal serpentinites using XANES spectroscopy. Earth. Planet. Sci. Lett. 466, 1–11.
Derbyshire, E.J., O'Driscoll, B., Lenaz, D., Gertisser, R., Kronz, A., 2013. Compositionally heterogeneous podiform chromitite in the Shetland Ophiolite Complex (Scotland): implications for chromitite petrogenesis and late stage alteration in the upper mantle portion of a supra-subduction zone ophiolite. Lithos 162–163, 279–300.
Eckstrand, O.D., 1975. The Dumont serpentinite: a model for control of nickeliferous opaque mineral assemblages by alteration reactions in ultramafic rocks. Econ. Geol. 70, 183–201.
Economou, M., Naldrett, A.J., 1984. Sulfides associated with podiform bodies of chromite at Tsangli Eretria, Greece. Miner. Deposita. 19, 289–297.
Fleet, M.E., Pan, Y., 1994. Fractional crystallization of anhydrous sulfide liquid in the system Fe-Ni-Cu-S, with application to magmatic sulfide deposits. Geochim. Cosmochim. Acta 58, 3369–3377.
Frezzotti, M.-L., Touret, J.L.R., 2014. CO_2, carbonate-rich melts, and brines in the mantle. Geos. Frontiers 5, 697–710.
Frost, B.R., 1985. On the stability of sulfides, oxides and native metals in serpentinite. J. Petrol. 26, 31–63.
Garuti, G., Pushkarev, E.V., Zaccarini, F., Cabella, R., Anikina, E., 2003. Chromite composition and platinum-group mineral assemblage in the Uktus Uralian–Alaskan-type complex (central Urals, Russia). Miner. Deposita. 38, 312–326.
Gervilla, F., Padro'n-Navarta, J.A., Kerestedjian, T., Sergeeva, I., González-Jiménez, J.M., Fanlo, I., 2012. Formation of ferrian chromite in podiform chromitites from the Golyamo Kamenyane serpentinite, Eastern Rhodopes, SE Bulgaria: a two stage process. Mineral. Petrol Contrib http://dx.doi.org/10.1007/.
Ghosh, B., Konar, R., 2011. Chromites from meta-anorthosites, Sittampundi layered igneous complex, southern India. J. Asia Earth Sci. 42, 1394–1402.
Ghosh, B., Konar, R., 2012. Textural developments in chromite deforming under eclogite facies conditions from the Neoarchaean Sittampundi anorthosite complex, southern India. Geol. J. 47, 253–262.
Ghosh, B., Morishita, T., Bhatta, K., 2013. Significance of chromian spinels from the mantle sequence of the Andaman Ophiolite, India: paleogeodynamic implications. Lithos 164–167, 86–96.
Ghosh, B., Ray, J., Morishita, T., 2014. Grain-scale plastic deformation of chromite from podiform chromitite of the Naga-Manipur ophiolite belt, India: implication for mantle dynamics. Ore. Gel. Rev. 56, 199–208.
Ghosh, B., Misra, S., Morishita, T., 2017. Plastic deformation and post-deformation annealing in chromite: mechanism and implications. Am. Mineral. 102, 216–226.
Gole, M.J., 2014. Leaching of S, Cu, and Fe from disseminated Ni-(Fe)-(Cu) sulphide ore during serpentinization of dunite host rocks at Mount Keith, Agnew-Wiluna belt, Western Australia. Miner. Deposita. 49, 821–842.
González-Jiménez, J.M., Gervilla, F., Griffin, W.L., Proenza, J.A., Augé, T., O'Reilly, S.Y., Pearson, N.J., 2012. Os-isotope variability within sulfides from podiform chromitites. Chem. Geol. 291, 224–235.
González-Jiménez, J.M., Griffin, W.L., Proenza, J.A., Gervilla, F., O'Reilly, S.Y., Akbulut, M., Pearson, N.J., Arai, S., 2014. Chromitites in ophiolites: How, where, when, why? Part II. The crystallization of chromitites. Lithos 189, 140–158.
González-Jiménez, J.M., Locmelis, M., Belousova, E., Griffin, William L., Gervilla, F., Kerestedjian, T., O'Reilly, S.Y., Sergeeva, I., Pearson, N.J., 2015. Genesis and tectonic implications of podiform chromitites in the metamorphosed Ultramafic Massif of Dobromirtsi (Bulgaria). Gondwana Res. 27, 555–574.
González-Jiménez, J.M., Barra, F., Garrido, L.N.F., Reich, M., Satsukawa, T., Romero, R., Salazar, E., Colás, V., Orellana, F., Rabbia, O., Plissart, G., Morata, D., 2016. A secondary precious and base metal mineralization in chromitites linked to the development of a Paleozoic accretionary complex in Central Chile. Ore Geol. Rev. 79, 14–40.
Gorring, M.L., Kay, S.M., 2000. Carbonatite metasomatized peridotite xenoliths from southern Patagonia: implications for lithospheric processes and Neogene plateau magmatism. Contrib. Mineral. Petrol. 140, 55–72.
Graham, I.T., Franklin, B.J., Marshall, B., 1996. Chemistry and mineralogy of podiform chromitite deposits, southern NSW, Australia: a guide to their origin and evolution. Mineral. Petrol. 37, 129–150.
Halfpenny, A., Prior, D.J., Wheeler, J., 2006. Analysis of dynamic recrystallization and nucleation in a quartzite mylonite. Tectonophysics 427, 3–14.
Haydoutov, I., Kolcheva, K., Daieva, L., Savov, I., 2001. Island arc origin of the Neoproterozoic variegated formations from East Rhodopes (Avren Synform and Bela Reka Antiform), Bulgaria. EUROPROBE Meeting, METU, Ankara, pp. 31–32 (Abstr).
Haydoutov, I., Kolcheva, K., Dieva, L.A., Savov, I., Carrigan, C., 2004. Island arc origin of the variegated formations from the east Rhodope, Bulgaria—implications for the evolution of the Rhodope Massif. Ofioliti 29 (2), 145–157.
Hey, M.H., 1954. A new review of the chlorites. Mineral. Mag. 30, 277–292.
Holwell, D.A., Keays, R.R., McDonald, I., Williams, M.R., 2015. Extreme enrichment of Se, Te, PGE and Au in Cu sulfide microdroplets: evidence from LA-ICP-MS analysis of sulphides in the Skaergaard Intrusion, east Greenland. Contrib. Mineral. Petrol. 170 (53).
Hughes, H.S.R., McDonald, I., Loocke, M., Butler, I.B., Upton, B.G.J., Faithfull, J.W., 2017. Paradoxical co-existing base metal sulphides in the mantle: the multi-event record preserved in Loch Roag peridotite xenoliths, North Atlantic Craton. Lithos 276, 103–121.
Ivanov, Z., 2000. Tectonic Position, Structure And Tectonic Evolution of Rhodope Massif. Guide. ABCD-GEODE, Bulgaria, pp. 1–4.
Jahn-Awe, S., Froitzheim, N., Nagel, T.J., Frei, D., Georgiev, N., Pleuger, J., 2010. Structural and geochronological evidence for Paleogene thrusting in the Western Rhodopes (SW Bulgaria): elements for a new tectonic model of the Rhodope Metamorphic Province. Tectonics 29, TC3008 (30 pp).
Janák, M., Froitzheim, N., Georgiev, N., Nagel, T.J., Sarov, S., 2011. P-T evolution of kyanite eclogite from the Pirin Mountains (SW Bulgaria): implications for the Rhodope UHP metamorphic complex. J. Met. Geol. 29, 317–332.
Kamenetsky, V.S., Kamenetsky, M.B., 2010. Magmatic fluids immiscible with silicate melts: examples from inclusions in phenocrysts and glasses, and implications for magma evolution and metal transport. Geofluids 10, 293–311.
Klein, F., Bach, W., 2009. Fe-Ni-Co-O-S phase relations in peridotite-seawater interactions. J. Petrol. 50, 37–59.
Kogarko, L., Henderson, C.M.B., Pacheco, H., 1995. Primary Ca-rich carbonate magma and carbonate–silicate–sulphide liquid immiscibility in the upper mantle. Contrib. Mineral., Petrol, pp. 121.
Kogarko, L., Kurat, G., Ntaflos, T., 2001. Carbonate metasomatism of the oceanic mantle beneath Fernando de Noronha Island, Brazil. Contrib. Mineral. Petrol. 140, 577–587.
Kolcheva, K., Haydoutov, I., Daieval, L., 2000. Dismembered ultramafic ophiolites from the Avren synform, Eastern Rhodopes. Geochem. Mineral. Petrology 37, 25–38.
Kozhoukharov, D., Kozhoukharova, E., Papanikolaou, D., 1988. Precambrian in the Rhodope massif. In: Zoubek, V. (Ed.), Precambrian in Younger Fold Belts: European Variscides, the Carpathians, and Balkans. International Geological Correlation Programme, Project 22. Wiley, Chichester, pp. 773–778.
Kozhoukharova, E., 1985. Origin and structural position of the serpentinised ultrabasic rocks from the Precambrian ophiolite association in Rhododpe Massif. III, Development stages and age of the ophiolite association. Geologica Balcanica 15 (5), 53–69 (in Russian).
Kozhoukharova, E., 1996. New data for the geological position of the Precambrian ophiolitic association in the Rhodope Massif. Comptes Rendus de l'Académie Bulgare des Sciences 49 (1), 57–60.
Kozhoukharova, E., 1998. Eclogitization of serpentinites into narrow shear zones from the Avren syncline, Eastern Rhodopes. Geochem. Mineral. Petrol. 35, 29–46 (in Bulgarian).
Kozhoukharova, E., 2010. Metaophiolite association in the Rhodope Massif as stratigraphical and structural marker. Scientific Annals, School o Geology, Aristotele Unversity of Thessaloniki, Proceedings of the XIX CBGA Congress, Thessaloniki, Greece. Special Volume, 100, pp. 165–171.
Kruse, R., Stünitz, H., 1999. Deformation mechanisms and phase distribution in mafic high temperature mylonites from the Jotun Nappe, southern Norway. Tectonophysics 303, 223–249.

Kullerud, G., Yund, R.A., Moh, G.H., 1969. Phase relations in the Cu–Fe–S, Cu–Ni–S, and Fe–Ni–S systems. In: Wilson, H.D.B. (Ed.), Magmatic Ore Deposits. Econ. Geol. Monograph 4, 323–343.
Leblanc, M., Nicolas, A., 1992. Ophiolitic chromitites. Int. Geol. Rev. 34 (7), 653–686.
Li, C., Barnes, S.-J., Makovicky, E., Rose-Hansen, J., Makovicky, M., 1996. Partitioning of nickel, copper, iridium, rhodium platinum and palladium between monosulphide solid solution and sulphide liquid: effects of composition and temperature. Geochim. Cosmochim. Acta 60, 1231–1238.
Liati, A., Gebauer, D., 1999. Constraining the prograde and retrograde P–T–t path of Eocene HP rocks by SHRIMP dating of different zircon domains: inferred rates of heating, burial, cooling and exhumation for central Rhodope, northern Greece. Contrib. Mineral. Petrol. 135, 340–354.
Liati, A., Gebauer, D., 2001. Alpine UHP rocks in the Rhodope zone N. Greece: evidence from exsolution textures in garnet-rich rocks. In: 6th International Eclogite Conference, pp. 76–77 (Abstract Volume).
Lord, R.A., Prichard, H.M., Sá, J.H.S., Neary, C.R., 2006. Chromite geochemistry and PGE fractionation in the Campo Formoso complex and Ipueira-Medrado sill, Bahia State, Brazil. Econ. Geol. 99 (2), 339–363.
Maier, W., Barnes, S.-J., 1996. Unusually high concentrations of magnetite at Caraíba and other Cu-sulfide deposits in the Curaçá Valley, Bahia, Brazil. Can. Mineral. 34, 717–731.
Marchev, P., Kaiser-Rhohrmeier, M., Heinrich, C.A., Ovtcharova, M., von Quadt, A., 2005. Hydrothermal ore deposits related to post-orogenic extensional magmatism and core complex formation: the Rhodope massif of Bulgaria and Greece. Ore Geol. Rev. 27, 53–89.
McGowan, N.M., Griffin, W.L., González-Jiménez, J.M., Belousova, E., Afonso, J.C., Shi, R., McCammon, C.A., Pearson, N.J., O'Reilly, S.Y., 2015. Tibetan chromitites: excavating the slab graveyard. Geology. https://doi.org/10.1130/G36245.1.
Mogessie, A., Scheipl, G., Bauer, C., Krenn, K., Georgieva, M., 2008. Petrology and Geochemistry of the Avren Complex, Rhodope Massif, Bulgaria. Abstract, International Geological Congress, Oslo.
Morishita, T., Maeda, J., Miyashita, S., Matsumoto, T., Dick, H., 2004. Magmatic srilankite (Ti_2ZrO_6) in gabbroic vein cutting oceanic peridotites: An unusual product of peridotite-melt interactions beneath slow-spreading ridges. Am. Mineral. 89, 759–766.
Morishita, T., Hattori, K.H., Terada, K., Matsumoto, T., Yamamoto, K., Takebe, M., Ishida, Y., Tamura, A., Arai, S., 2008. Geochemistry of apatite-rich layers in the Finero phlogopite–peridotite massif (Italian Western Alps) and ion microprobe dating of apatite. Chem. Geol. 251, 99–111.
Mountain, B.W., Wood, S.A., 1988. Chemical controls on the solubility, transport and deposition of platinum and palladium in hydrothermal solutions: a thermodynamic approach. Econ. Geol. 83 (492), 511.
Mposkos, E., 1998. Cretaceous and tertiary tectonometamorphic events in Rhodope zone (Greece): petrological and geochronological evidences. Bull. Geol. Soc. Greece 32, 59–67.
Mposkos, E., 2002. Petrology of the ultrahigh pressure metamorphic Kimi complex in Rhodope (NE Greece): a new insight into the Alpine geodynamic evolution of the Rhodope. Bull. Geol. Soc. Greece 34, 2126–2188.
Mposkos, E., Krohe, A., 2000. Petrological and structural evolution of continental high pressure (HP) metamorphic rocks in the Alpine Rhodope Domain (N. Greece). In: Panaydes, I., Xenopontos, C., Malpas, J. (Eds.), Proceedings of the 3rd International Conference on the Geology of the Eastern Mediterranean (Nicosia, Cyprus). Geol. Surv. Cyprus, pp. 221–232.
Mposkos, E., Krohe, A., 2006. Pressure–temperature–deformation paths of closely associated ultra-high-pressure (diamond-bearing) crustal and mantle rocks of the Kimi complex: implications for the tectonic history of the Rhodope Mountains, northern Greece. Can. J. Earth Sci. 43, 1755–1776.
Mposkos, E., Liati, A., 1993. Metamorphic evolution of metapelites in the high-pressure terrane of the Rhodope Zone, Northern Greece. Can. Mineral. 31, 401–424.
Mposkos, E., Baziotis, I., Proyer, A., 2012. Pressure–temperature evolution of eclogites from the Kechros complex in the Eastern Rhodope (NE Greece). Int. J. Earth Sci. 101 (4), 973–996.
Mukasa, S., Haydoutov, I., Carrigan, C., Kolcheva, K., 2003. Thermobarometry and 40Ar39Ar ages of eclogitic and gneissic rocks in the Sredna Gora and Rhodope terranes of Bulgaria. J. Czech Geol. Soc. 48, 94–95.
Mukherjee, R., Mondal, S.K., Rosing, M.T., Frei, R., 2010. Compositional variations in the Mesoarchean chromites of the Nuggihalli schist belt, Western Dharwar Craton (India): potential parental melts and implications for tectonic setting. Contrib. Mineral. Petrol. 160 (6), 865–885.
Mungall, J., Andrews, D.R., Cabri, L.J., Sylvester, P., Rubrett, M., 2005. Partitioning of Cu, Ni, Au, and platinum-group elements between monosulfide solid solution and sulfide under controlled oxygen and sulfur fugacities. Geochim. Cosmochim. Acta 69, 4349–4360.
Nagel, T.J., Schmidt, S., Janak, M., Froitzheim, N., Jahn-Awe, S., Georgiev, N., 2011. The exposed base of a collapsing wedge: The Nestos Shear Zone (Rhodope Metamorphic Province, Greece). Tectonics 30, TC4009. https://doi.org/10.1029/2010TC002815.
Naldrett, A., Duke, J.M., 1980. Pt metals in magmatic sulfide ores. Science 208, 1417–1424.
Naldrett, A.J., Lehmann, J., Augé, T., 1989. Spinel non-stoichiometry and reactions between chromite and closely associated sulphides, with examples from ophiolite complexes. In: Predergast, M.D., Jones, J. (Eds.), Magmatic sulphides-the Zimbabwe volume. The Institution of Mining and Metallurgy, London, pp. 221–227.
Naldrett, A.J., 2010. Secular variation of magmatic sulfide deposits and their source magmas. Econ. Geol. 105, 669–688.
Naldrett, A.J., Wilson, A., Kinnaird, J., Yudovskaya, M., Chunnett, G., 2012. The origin of chromitites and related PGE mineralization in the Bushveld Complex: new mineralogical and petrological constraints. Mineral. Deposita. 47 (3), 209–232.
Neigishi, H., Arai, S., Yurimoto, H., Ito, S., Ishimaru, S., Tamura, A., Akizawa, N., 2013. Sulfide-rich dunite within a thick Moho transition zone of the northern Oman ophiolite: implications for the origin of Cyprus-type sulfide deposits. Lithos 164–167, 22–35.
O'Driscoll, B., González-Jiménez, J.M., 2016. Petrogenesis of the platinum-group minerals. Rev. Mineral. Geochem. 81, 489–578.
Pannina, L.I., Motorina, I.V., 2008. Liquid immiscibility in deep-seated magmas and the generation of carbonatite melts. Geochem. Int. 46, 448–464.
Passchier, C.W., Trouw, R.A.J., 2005. Microtectonics, second ed. Springer, Berlin, Heidelberg, New York.
Peregoedova, A.V., Barnes, S.J., Baker, D.R., 2004. The formation of Pt–Ir alloys and Cu–Pd-rich sulfide melts by partial desulfurization of Fe–Ni–Cu sulfides: results of experiments and implications for natural systems. Chem. Geol. 208, 247–264.
Peytcheva, I., von Quat, A., Ovtcharova, M., Handler, R., Neubauer, F., Salnikova, E., Kostitsyn, Y., Sarov, S., Kolcheva, K., 2004. Metagranitoids from the eastern part of the Central Rhodopean Dome (Bulgaria): U-Pb, Rb–Sr and $^{40}Ar/^{39}Ar$ timing of emplacement and exhumation and isotope-geochemical features. Mineral. Petrol. 82, 1–31.
Piña, R., Gervilla, F., Barnes, S.J., Ortega, L., Lunar, R., 2012. Distribution of platinum-group and chalcophile elements in the Aguablanca Ni–Cu sulfide deposit (SW Spain): evidence from a LA-ICP-MS study. Chem. Geol. 302–303, 61–75.
Prichard, H.M., Lord, R.A., 1993. An overview of the PGE concentrations in the Shetland ophiolite complex. In: Prichard, H.M., Alabaster, T., Harris, N.B.W., Neary, C.R. (Eds.), Magmatic Processes and Plate Tectonics. Geol. Soc. Spec. Publ., pp. 273–294.
Prichard, H.M., Neary, C.R., Fisher, P.C., O'Hara, M.J.O., 2008. PGE-rich podiform chromitites in the Al'Ays ophiolites complex, Saudi Arabia: an example of critical mantle melting to extract and concentrate PGE. Econ. Geol. 103, 1507–1529.
Proenza, J.A., Gervilla, F., Melgarejo, J.C., Vera, O., Alfonso, P., Fallick, A., 2001. Genesis of sulfide-rich chromite ores by the interaction between chromitite and olivine-norite dikes in the Potosí Mine (Moa-Baracoa ophiolitic massif, eastern Cuba). Miner. Deposita. 36, 658–669.
Proenza, J.A., Zaccarini, F., Lewis, J.F., Longo, F., Garuti, G., 2007. Chromian spinel composition and the platinum-group minerals of the PGE-rich Loma Peguera chromitites, Loma Caribe peridotite, Dominican Republic. Can. Mineral. 45, 631–648.
Ricou, L.E., Burg, J.P., Godfiaux, I., Ivanov, Z., 1998. Rhodope and Vardar: the metamorphic and the olistostromic paired belts related to the Cretaceous subduction under Europe. Geodinamica Acta 11 (6), 285–309.
Rosière, C., Siemes, H., Quade, H., Brokmeier, H.-G., Jansen, E.M., 2001. Microstructures, textures and deformation mechanisms in hematite. J. Str. Geol. 23, 1429–1440. https://doi.org/10.1016/S0191-8141(01)00009-8.
Satsukawa, T., Piazolo, S., González-Jiménez, J.M., Colás, V., O'Reilly, S.Y., Gervilla, F., Fanlo, I., Kerestedjian, T.N., 2015. Fluid-present deformation aids chemical modification of chromite: insights from chromite from Golyamo Kamneyane, SE Bulgaria. Lithos 228–229, 78–89.
Sciortino, M., 2014. Generation of High-Ni Sulfide and Alloy Phase During Serpentinization of the Dumont Dunite, Quebec (Ph.D. thesis). University of Toronto, pp. 87.
Tarkian, M., Nadienova, E., Zhelyaskova-Panayotova, M., 1991. Platinum-group minerals in chromitites from the eastern Rhodope ultramafic complex, Bulgaria. Mineral. Petrol. 44, 73–87.
Thalhammer, O.A.R., Prochaska, W., Mühlhans, H.W., 1990. Solid inclusions in chromespinels and platinum group element concentration from the Hochgrössen and Kraubath Ultramafic Massifs (Austria). Contrib. Mineral. Petrol. 105, 66–80.
Turpaud, P., Reischmann, T., 2010. Characterisation of igneous terranes by zircon dating: implications for UHP occurrences and suture identification in the Central Rhodope, northern Greece. Int. J. Earth Sci. 99 (3), 567–591.
Ueno, T., Ito, Sh.-I., Nalatsuka, Sh., Nakano, K., Harada, T., Yamazaki, T., 2000. Phase equilibria in the system Fe-Ni-S at 500 °C and 400 °C. J. Mineral. Petrol. Sci. 95, 145–161.
Urai, J., Means, W.D., Lister, G.S., 1986. Dynamic recrystallization of minerals. In: Heard, H.C., Hobbs, B.E. (Eds.), Mineral and Rock Deformation: Laboratory Studies, the Paterson Volume. Geophys. Monogr 36. Am. Geophys. Union, Washington DC, pp. 161–200.
Zaccarini, F., Stumpfl, E.F., Garuti, G., 2004. Zirconolite and Zr–Th–U minerals in chromitites of the Finero Complex, western Alps, Italy: evidence for carbonatite type metasomatism in a subcontinental mantle plume. Can. Mineral. 42 (6), 1825–1845.
Zhelyaskova-Panayotova, M., Zinzov, Z., Pashov, V., 2000. Hydrothermal gold mineralization in ultrabasites near Dobromirtsi village, Kurdjali region. Annuarie Université de Sofia 93, 173–186.